

**MASTER**

**Modelling and identification of a laser deflecting system**

Slots, T.D.

*Award date:*  
1994

[Link to publication](#)

**Disclaimer**

This document contains a student thesis (bachelor's or master's), as authored by a student at Eindhoven University of Technology. Student theses are made available in the TU/e repository upon obtaining the required degree. The grade received is not published on the document as presented in the repository. The required complexity or quality of research of student theses may vary by program, and the required minimum study period may vary in duration.

**General rights**

Copyright and moral rights for the publications made accessible in the public portal are retained by the authors and/or other copyright owners and it is a condition of accessing publications that users recognise and abide by the legal requirements associated with these rights.

- Users may download and print one copy of any publication from the public portal for the purpose of private study or research.
- You may not further distribute the material or use it for any profit-making activity or commercial gain

7194

EINDHOVEN UNIVERSITY OF TECHNOLOGY  
DEPARTMENT OF ELECTRICAL ENGINEERING  
Measurement and Control Section

## **Modelling and identification of a laser deflecting system**

by T.D. Slots

M. Sc. Thesis on Practical training period  
carried out from February 1994 to August 1994  
commissioned by Prof. Dr. Ir. P.P.J. van den Bosch  
under supervision of Dr. Ir. A.A.H. Damen and Ing. R.A. Zorge  
date: August 1994

The Department of Electrical Engineering of the Eindhoven University of Technology accepts no responsibility for the contents of M.Sc. Theses or reports on practical training periods.

## Summary

In the measurement and control section a laser deflecting system has been designed. The system consists of a hemispherical mirror in an air bearing, allowing it to rotate. A control system keeps the air gap between the mirror and the bearing system constant.

Three arms are attached to the mirror, at angles of  $120^\circ$ . The arms are directed slightly upwards from the mirror surface, at an angle of  $15^\circ$ . Attached on the arms by very stiff strings are three actuators. The actuators work on the mirror arms on the same principle as music speakers; activating a coil in a magnetic induction field. This way the actuators can move frictionless. The actuators are attached to the base of the system by springs. The purpose of these strings is to put pretensioning on the mirror.

The goal of this research is to gain insight in the behaviour of the deflecting system and to model and identify the dynamics of the system. The modeling and identification of the deflecting system serve the ultimate goal of designing a controller to manipulate the movements of the mirror, so it can be used for tracking purposes.

The position of the system is described using Bryant angles. With these a non-linear differential equation is derived describing the dynamics of the system.

The non-linear differential equation is linearized to obtain a linear model. The sensors of the system are designed in a way that the normal of the surface of the mirror can be measured. The rotation of the mirror around the normal cannot be measured. In the linearized model, the rotation round the normal of the mirror is not expressed. The linear model consists of two SISO systems, describing two angles of the mirror. With these angles the normal can be calculated.

At the time of this research the system was undergoing alterations, so the real system was not available for the identification. A simulation of the mirror control is implemented in the Simulab environment of Matlab, based on the non-linear differential equation using Bryant angles. Two of the Bryant angles describe the position of the normal to the mirror. The third describes the rotation round the normal. Rotation round the normal does not directly influence the normal, but it influences the dynamics of the system, and so influencing the other Bryant angles and thus the normal.

The simulation is used to provide the input and output dataset for the identification. The input to the system is a noise series. From the generated data a MIMO model has been identified.

The identified model describes two angles defining the normal of the mirror. These angles are the same as those measured by the sensors. The model has been validated by a second dataset from the simulation, again with a noise series as input. The model describes the system well.

<b>1. Introduction</b>	<b>4</b>
<b>2. System description</b>	<b>6</b>
2.1 Mirror description	8
2.1.1 Mirror orientation	8
2.1.2 The mirror sensor	9
2.2 Actuator description	12
2.2.1 Actuator force using current control	12
2.2.2 Actuator force using voltage control	13
<b>3. System dynamics</b>	<b>14</b>
3.1 Mirror dynamics	15
3.2 Actuator dynamics	17
<b>4. Model linearization</b>	<b>19</b>
4.1 Linearizing string force magnitude $F_i$	20
4.2 Linearizing the string force direction $\underline{d}_i$	22
4.3 The momentum $\underline{M}_1$ on arm 1	22
4.4 The momentum $\underline{M}_2$ on arm 2	24
4.5 The momentum $\underline{M}_3$ on arm 3	26
4.6 The total momentum $\underline{M}_0$ on the mirror	27
4.7 The linear system description	28
4.8 Linear characteristics	31
4.8.1 Pole placement	31
4.8.2 Step responses	32
4.8.3 Bode plots of the linear model	33
<b>5. System simulation</b>	<b>35</b>
5.1 Simulation characteristics	36
5.1.1 Step responses of each actuator	37
5.1.2 Step responses using $U_\psi$ and $U_\theta$	38
5.1.3 Comparing the linear system with the simulation	39
<b>6. Identification of the simulation</b>	<b>41</b>
6.1 Model structure and the minimization criterion	42

6.2 Experiment design	43
6.2.1 Data collection sample frequency	43
6.2.2 Identification sample frequency $f_s$	43
6.2.3 Determining experiment duration	44
6.3 Data preprocessing	44
6.3.1 Sample rate reduction	44
6.3.2 Detrending and peak shaving	44
6.3.3 Delay time correction	44
6.3.4 Signal scaling	45
6.4 Model estimation	45
6.5 Model validation	45
6.5.1 Correlation between inputs and residuals	45
6.5.2 Comparing real and estimated output	45
<b>7. Identification results</b>	<b>46</b>
7.1 Data preprocessing	46
7.1.1 Peakshaving and detrending	47
7.1.2 Delay time correction	47
7.1.3 Sample rate reduction to $f_s$ and normalization	48
7.1.4 Equal variance scaling	48
7.2 Model estimation	49
7.3 Model validation	52
7.4 Siso model validation	56
<b>8. Conclusions</b>	<b>58</b>
Appendix A: Transforming the local normal coordinates to global coordinates using sensor angles	60
Appendix B: Calculation of $\underline{a}_i$ , $\underline{\Delta}_i$ and $\underline{B}_i$	62
Appendix C: The simulation blocks	64
Appendix D: Notes on running simulations in Simulink	68
Appendix E: Matlab M-files	69

# 1. Introduction

The Measurement and Control section of the Department of Electrical Engineering of the Eindhoven University of Technology finds study topics in the measurement, identification and control of processes. The Measurement and Control section has several laboratory processes on which theoretical strategies can be tested and developed.

One of the laboratory processes is a laser deflecting system. Intended use of this system is tracking purposes in flexible automation, for example to track the tool center point (TCP) of a robot. In Figure 1.1 a schematic view of such a tracking system is shown.

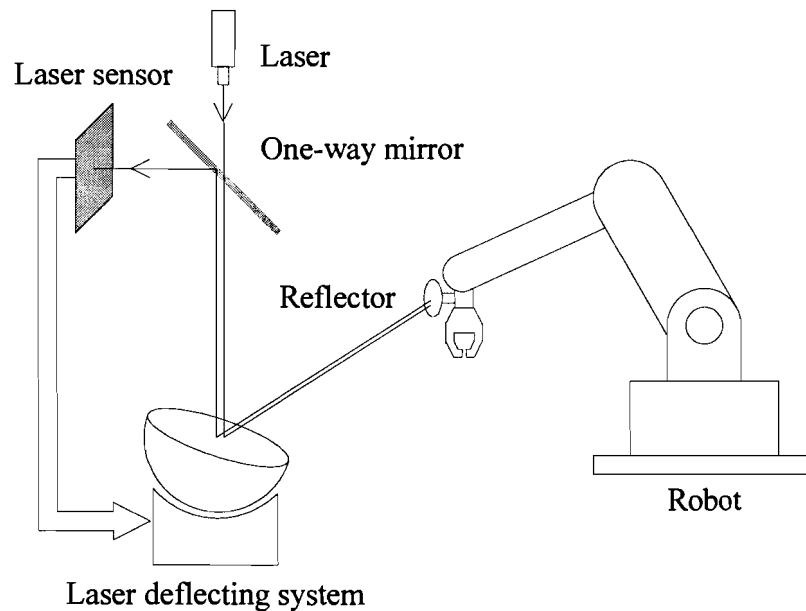


Figure 1.1: Schematic view of a laser tracking system.

In Figure 1.1 a laser beam is passed through a half-way mirror and deflected on the laser deflecting system. The deflecting system aims the laser beam on a special reflector fixed on the TCP of a robot. The laser beam is reflected back parallel to the incoming beam. The beam follows the same path back until it is bounced off the half-way mirror and comes onto the laser sensor. The sensor information is led into the deflecting system. The orientation of the deflecting system can then be adjusted to follow the TCP of the robot.

The position of the TCP can be calculated using two deflecting systems, or by using one deflecting system together with the distance information of the TCP. The distance information can be obtained by modulating the laser. By analyzing the phase shift of the returning laser beam the distance information can be obtained.

The laser deflecting system consists of a hemispherical air bearing: a half circle bearing acting as a mirror in a bearing seat. The mirror can be positioned through three actuators.

A preliminary study of the deflecting system has been done by the faculty of Mechanical Engineering, see [5].

During this research the laser deflecting system was in revision. The goal of the research is to gain insight in the laser deflecting system, so a controller for the positioning of the mirror can be developed and later tested on the real system.

For this purpose a simulation model will be designed. The simulation data will be used to identify the system, and based upon that a controller can be designed.

## 2. System description

The laser deflecting system consists of a hemispherical air bearing. A schematic view of the laser deflecting system is shown in Figure 2.1. Three arms are attached to the mirror. These arms are attached to the actuators by stiff strings. Each string is fixed with joints, indicated in Figure 2.1 by dots. The actuator is a coil moving in air along its core. The core is fixed to the

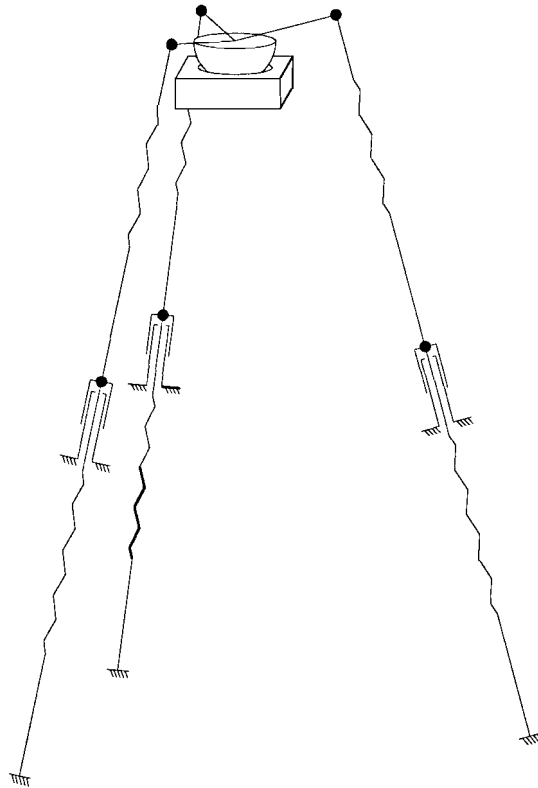


Figure 2.1: Schematic view of the laser deflecting system.

base of the system. This means that the actuator can only move in a straight line. The actuator is fixed to the base of the system with a spring. The spring is used for pretensioning the mirror.

Air is blown from below into the bearing seat. This causes the mirror to float on an air cushion. To maintain a constant gap between the mirror and the seat, a control system is designed. The control system acts upon the actuators, controlling the gap.

The assumption is made that the gap between the mirror and the bearing seat is constant, consequently the mirror can only rotate in the seat. The center of rotation is the middle of the sphere of which the mirror is a half.

Two frames can be defined: a global frame and a local frame.

The global frame is fixed to the base of the system. The origin of the global frame is the center of rotation of the mirror.

The local frame is fixed to the surface of the mirror, moving along with the movements of the mirror. The origin of the local frame is also the center of rotation of the mirror. When the



mirror is not rotated, both frames coincide. The Cartesian coordinate system will be used for both frames.

The coordinates of a vector defined in the global frame will be given the subscript G, the coordinates of a vector in the local frame will be given no subscript. The orientation of the mirror with respect to both frames is depicted in Figure 2.2. In Figure 2.2 the mirror is not

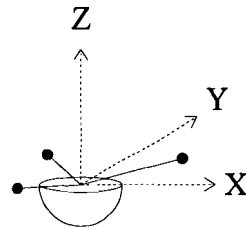


Figure 2.2: Orientation of the mirror.

rotated and the y-axis is directed into the page.

Note that the arms are physically non-existent to avoid interference with the laser beam. The connections of the strings to the mirror have been realized by a framework at the edge of the mirror.

## 2.1 Mirror description

The arms of the mirror are positioned at an angle of  $120^\circ$  between each other. Each arm is positioned at an angle of  $15^\circ$  to the surface of the mirror. Top and side views of the mirror are shown in Figure 2.3. The arm numbering is also shown in Figure 2.3.

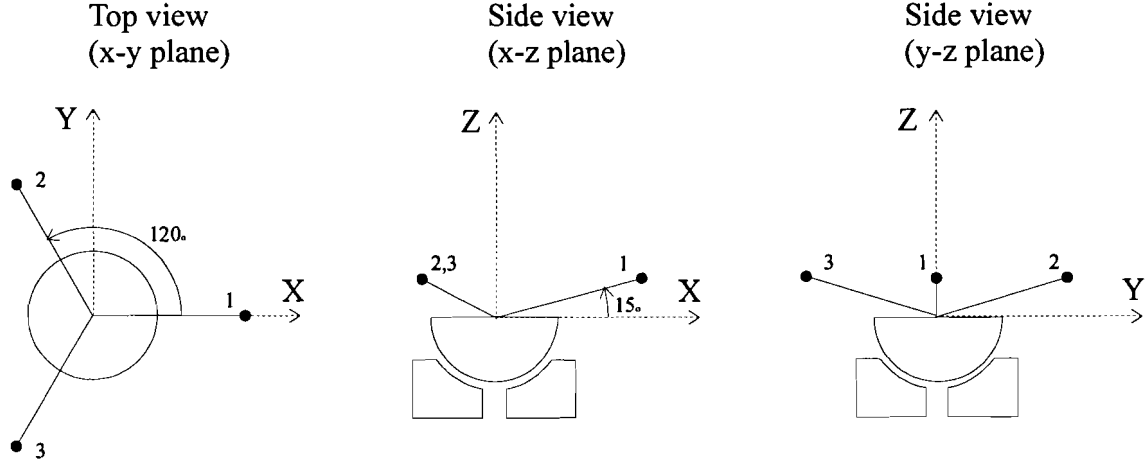


Figure 2.3: Top and side views of the mirror.

### 2.1.1 Mirror orientation

To determine the orientation of the local and global frame to each other, Bryant angles will be used. With the use of the Bryant angles, the coordinates of a vector can be transformed from one frame to the other [8]. The Bryant angles are angles of rotations transforming the global base to the local base. The Bryant angles used here are  $\psi$ ,  $\theta$  and  $\phi$ . The transformation is displayed in Figure 2.4.

First the global frame is rotated round the x-axis, the angle of rotation is  $\psi$ . This results in the frame  $X_G'$ ,  $Y_G'$ ,  $Z_G'$ . This frame is rotated round  $Y_G'$ , with angle  $\theta$ , resulting in the frame  $X_G''$ ,  $Y_G''$ ,  $Z_G''$ . Finally this frame is rotated round  $Z_G''$ , with angle  $\phi$ . All rotations are directed around the positive axes. The result is the frame  $X_G'''$ ,  $Y_G'''$ ,  $Z_G'''$ . This frame is the local frame  $X$ ,  $Y$ ,  $Z$ . If a vector defined in local coordinates  $\underline{\epsilon}=[x \ y \ z]^T$  is taken, then the coordinates of this vector can be transformed to global coordinates, using the transformation matrix  $R_B$ :

$$\begin{bmatrix} x_G \\ y_G \\ z_G \end{bmatrix} = R_B \cdot \begin{bmatrix} x \\ y \\ z \end{bmatrix} \quad (2.1)$$

With the transformation matrix  $R_B$  [8]:

$$R_B = \begin{bmatrix} \cos(\theta)\cos(\phi) & -\cos(\theta)\sin(\phi) & \sin(\theta) \\ \cos(\psi)\sin(\phi) + \sin(\psi)\sin(\theta)\cos(\phi) & \cos(\psi)\cos(\phi) - \sin(\psi)\sin(\theta)\sin(\phi) & -\sin(\psi)\cos(\theta) \\ \sin(\psi)\sin(\phi) - \cos(\psi)\sin(\theta)\cos(\phi) & \sin(\psi)\cos(\phi) + \cos(\psi)\sin(\theta)\sin(\phi) & \cos(\psi)\cos(\theta) \end{bmatrix} \quad (2.2)$$

The inverse matrix of  $R_B$  is simply  $R_B^T$ , since  $R_B$  is an orthonormal matrix:  $R_B^T \cdot R_B = I$ . The coordinates of a vector can be transformed from global to local frame coordinates using  $R_B^T$ , in the same way as in (2.1). If the Bryant angles are known, the exact position of the mirror

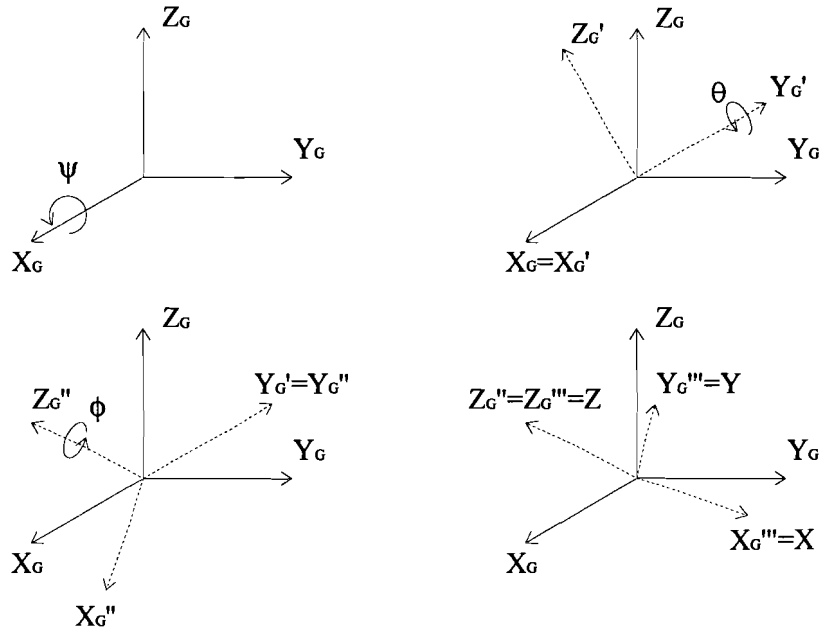


Figure 2.4: Transformation from the global to the local frame using Bryant angles.

relative to the global frame is known. The vector  $\gamma$  is defined as a vector containing the Bryant angles:  $\gamma = [\psi \ \theta \ \phi]^T$ .

### 2.1.2 The mirror sensor

The laser deflecting system will be used to aim a laser beam. The normal of the mirror surface defines the way the laser beam is deflected. The angle of the normal to the z-axis of the global frame is limited to  $26^\circ$ . This limits the range of the deflecting system. Three coils are fixed to the system to determine the position of the normal. One coil is fixed to the mirror, and two coils are fixed to the base of the system. A top and two side views are shown in Figure 2.6. The base coils are positioned at an angle of  $45^\circ$  to the x and y axes. An alternating current  $I$  is led through the mirror coil. This causes a magnetic induction  $\underline{B}$ . The contribution of the length  $d\underline{l}$  of a coil winding to the magnetic induction is  $d\underline{B}$ . If the vector from  $d\underline{l}$  to  $d\underline{B}$  is  $\underline{r}$  then for  $d\underline{B}$  can be written [9] (see Figure 2.5):

$$d\underline{B} = \frac{\mu_0}{4\pi} I \frac{d\underline{l} \times \underline{r}}{r^3} \quad (2.3)$$

In (2.3)  $\mu_0$  is the magnetic permeability of vacuum. In the first side view of Figure 2.6 the mirror is not tilted, and only one base coil is depicted. The magnetic flux  $\phi_m$  is give by (2.4).

$$\phi_m = \iint_A \underline{B} \cdot \underline{n} dA \quad (2.4)$$

It can easily be seen that there is no resulting flux through the base coil in the first side view. The second side view shows the mirror tilted  $30^\circ$ . The resulting flux through the base coil is again given by (2.4) The flux is not zero now, and causes a current to flow through the base

coil. The current through the base coil is a measure of how much the mirror is tilted. The same

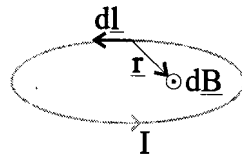


Figure 2.5: The magnetic induction.

principle can be applied to the other base coil. Both current signals from the base coils are processed, and the resulting sensor signal gives information about the position of the normal vector to the mirror's surface. The sensor gives the angles  $\alpha$  and  $\beta$ , see Figure 2.7. The normal  $\underline{n}$  of the mirror is projected to the  $yz$  and  $xz$  plane of the global frame. The angle of the  $yz$  projection to the  $z$ -axis is  $\alpha$ , and the angle of the  $xz$  projection to the  $z$ -axis is  $\beta$ .  $\alpha$  is positive if  $Y_G$  is negative, and  $\beta$  is positive if  $X_G$  is positive.

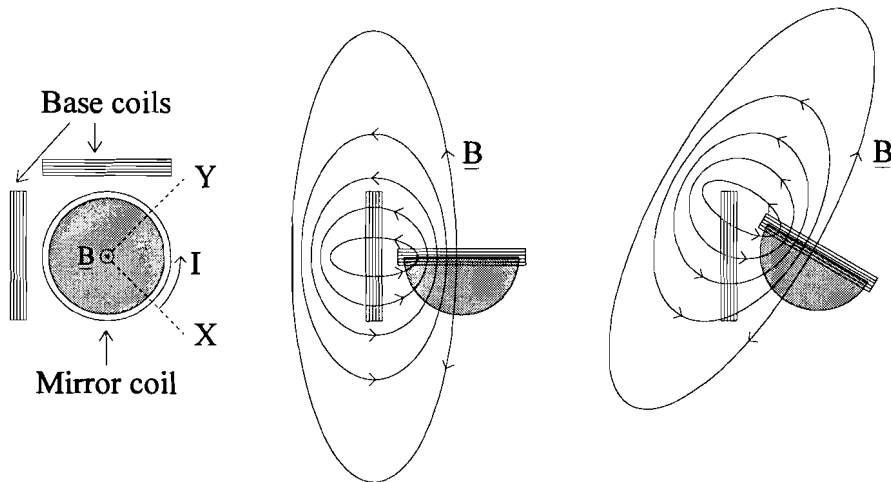


Figure 2.6: The mirror sensor.

No research has been done to find the current through the base coils as a function of how the mirror is tilted, nor how the current signals should be processed to get angles  $\alpha$  and  $\beta$ .

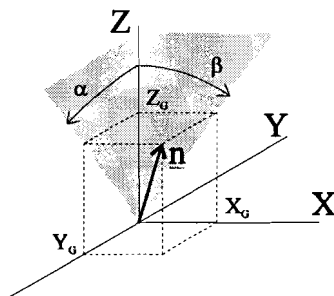


Figure 2.7: Sensor angles.

The sensor angles define the position of the normal to the mirror, but they do not define the position of the mirror itself: the rotation of the mirror around the normal is not expressed through  $\alpha$  and  $\beta$ . Rotation of the mirror around its normal does not effect the path of the laser beam, but does effect the resulting momentum on the mirror, and by doing so the dynamics of the mirror. The dynamics of the mirror can therefore not be described using only the sensor angles.

The rotation round the normal is given by  $\phi$  when using Bryant angles. This means the sensor angles can be described by the Bryant angles  $\psi$  and  $\theta$ . The normal to the mirror given in local coordinates is:  $\underline{n}=[0 \ 0 \ 1]^T$ . The coordinates in global coordinates are:

$$\begin{bmatrix} X_G \\ Y_G \\ Z_G \end{bmatrix}_n = R_B \cdot \begin{bmatrix} 0 \\ 0 \\ 1 \end{bmatrix} = \begin{bmatrix} \sin(\theta) \\ -\sin(\psi) \cos(\theta) \\ \cos(\psi) \cos(\theta) \end{bmatrix} \quad (2.5)$$

If the sensor angles are used (see appendix A):

$$\begin{bmatrix} X_G \\ Y_G \\ Z_G \end{bmatrix}_n = \frac{1}{\sqrt{1 + \cos^2(\beta) \tan^2(\alpha)}} \begin{bmatrix} \sin(\beta) \\ -\tan(\alpha) \cos(\beta) \\ \cos(\beta) \end{bmatrix} \quad (2.6)$$

If (2.5) and (2.6) are equalized the angles become:

$$\psi = \alpha$$

$$\theta = \sin^{-1} \left( \frac{1}{\sqrt{1 + \cos^2(\beta) \tan^2(\alpha)}} \sin(\beta) \right)$$

And: (2.7)

$$\alpha = \psi$$

$$\beta = \tan^{-1} \left( \frac{\tan(\theta)}{\cos(\psi)} \right)$$

With (2.7) the sensor and Bryant angles can be transformed from and to each other.

## 2.2 Actuator description

The actuator works on the same principle as a speaker. The actuator is shown in Figure 2.8.

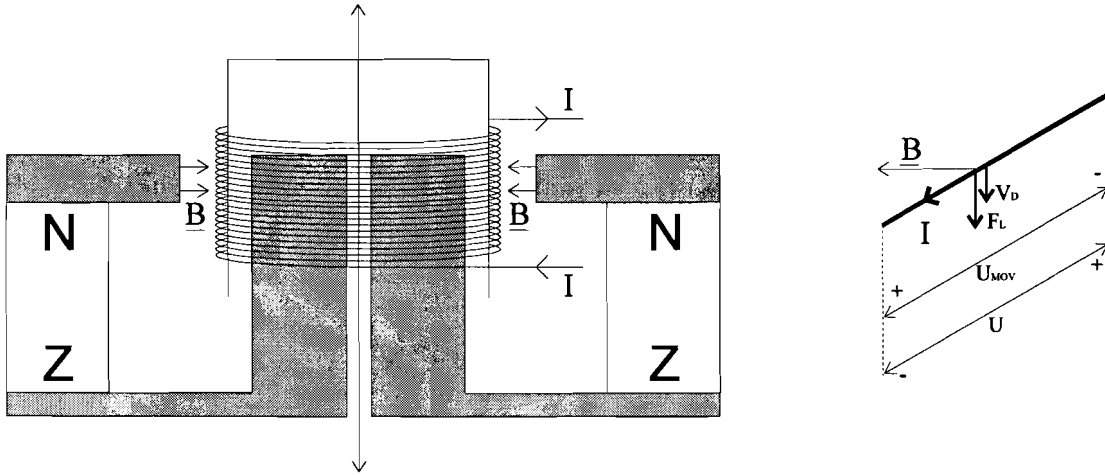


Figure 2.8: The actuator.

A permanent magnet produces a magnetic field with induction  $\underline{B}$  between the core and upper magnetic conductor. This induction is assumed to be constant in the gap. A coil can move in the gap. The coil is wound on a cylinder connected to the stiff string, and the pretensioning spring. The string is connected to a mirror arm and the pretensioning spring is connected to the base of the system.

### 2.2.1 Actuator force using current control

If a charge  $q$  moves through a magnetic field with induction  $\underline{B}$  and speed  $\underline{v}$ , a Lorentz force is exercised on the charge [9]:

$$\underline{F}_L = q\underline{v} \times \underline{B} \quad (2.8)$$

In the case drawn in the right plot of Figure 2.8, the Lorentz force is always directed downwards, and exercised on the actuator coil. For this force can be written:

$$F_L = I \int_0^l B dl = IBl \quad (2.9)$$

If the coil has radius  $r$ , and there are  $N$  windings in the magnetic field (2.9) becomes:

$$F_L = 2\pi r N I B \quad (2.10)$$

If the current is reversed, the force is directed upwards.  $F_A$  is the actuator force caused by a current  $I$ .  $F_A$  is defined positive upwards, and  $I$  is defined positive as indicated in Figure 2.8. For the actuator force is found:

$$F_A = -2\pi r N I B = -AI \quad (2.11)$$

And therefore for the actuator constant A by definition:

$$A = 2\pi rNB \quad (2.12)$$

### 2.2.2 Actuator force using voltage control

A voltage U is now put on the coil. In the right plot of Figure 2.8 a piece off coil is shown. The voltage causes a current to flow through the coil, in its turn causing a Lorentz force downwards. If the Lorentz force causes the coil to move downwards with speed  $V_D$ , an induction voltage  $U_{MOV}$  is generated by the movement [9].  $U_{MOV}$  is directed opposite of the externally applied voltage U. If the coil has resistance R and inductance L the following is found [9]:

$$U - U_{MOV} = RI + L\dot{I} \quad (2.13)$$

$U_{MOV}$  is caused by the movement of the charge in the coil through  $\underline{B}$ . For  $U_{MOV}$  can be found: [9]:

$$U_{MOV} = V_D Bl = 2\pi rNV_D B = AV_D \quad (2.14)$$

The position of the coil will be given by  $h_A$ .  $h_A$  is the position of the coil from the equilibrium position, and is positive directed upwards along the actuator core. This means:

$$V_D = -\dot{h}_A \quad (2.15)$$

By substituting (2.15) and (2.14) in (2.13) the following is found using the Laplace notation:

$$U + sAh_A = RI + sLI \Rightarrow$$

$$I = \frac{U + sAh_A}{R + sL} \quad (2.16)$$

The actuator force is found by substituting (2.11) in (2.16) and is a function of the applied voltage U and of the actuator position  $h_A$ :

$$F_A = \frac{-AU - sA^2h_A}{R + sL} \quad (2.17)$$

### 3. System dynamics

In this chapter the dynamics of the system will be discussed. For this purpose the dynamics of the mirror and the actuator are treated separately. First the variables and parameters will be discussed.

In Figure 3.1 the mirror with one actuator is shown.

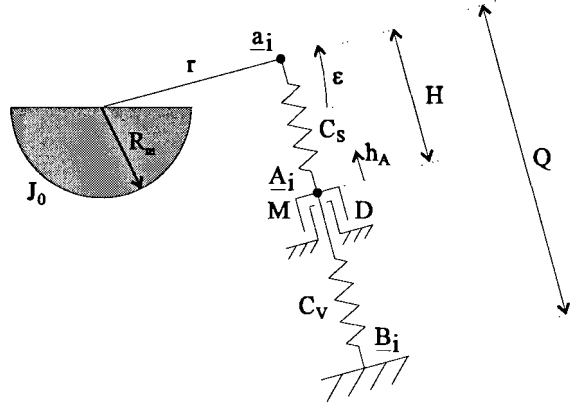


Figure 3.1: Mirror with one actuator arm.

The meaning of the abbreviations will now be described.

$r$  : Length of the arm attached to the mirror.

$R_m$  : Radius of the mirror half sphere

$H$  : Length of the string connecting the mirror arm and the actuator.  $H$  is the equilibrium length.

$Q$  : Length of the string and spring together.  $Q$  is the equilibrium length.

$M$  : Mass of the actuator coil.

$C_s$  : Spring constant of the stiff string.

$C_v$  : Spring constant of the pretensioning string.

$D$  : Damping between the actuator and base.

$J_0$  : Inertia matrix of the rotations around the local frame axes.  $J_0$  has been calculated in [5]:

$$J_0 = \begin{bmatrix} \frac{1}{5}mR_m^2 & 0 & 0 \\ 0 & \frac{1}{5}mR_m^2 & 0 \\ 0 & 0 & \frac{1}{5}mR_m^2 \end{bmatrix} = \frac{1}{5}mR_m^2 \cdot I = j_0 \cdot I$$

In this equation  $m$  is the mass of the half mirror sphere.

$\epsilon$  : Angle of any mirror arm to the mirror surface.

$\underline{a}_i$  : Vector to end of mirror arm number  $i$ .  $\underline{a}_i$  is defined as:  $\underline{a}_i = [x \ y \ z]^T_i$ . This vector is constant if defined in local coordinates.

$\underline{A}_i$  : Vector to actuator number  $i$ . Actuator  $i$  is the actuator on arm  $i$ .

$\underline{B}_i$  : Vector to the base of the system where the spring is connected.  $\underline{B}_i$  is defined as:  $\underline{B}_i = [X \ Y \ Z]^T_i$ , with  $[X \ Y \ Z]^T_i = R_B^T \cdot [X_G \ Y_G \ Z_G]^T_i$ . This vector is constant if defined in global coordinates.

$h_A$  : Movement from the equilibrium position off the actuator along the actuator core.  $h_A$  is positive upwards along the core. In the subscript an  $i$  is added to indicate the movement of the different actuators.



The following actuator variables are not shown in Figure 3.1:

- A : Coil constant, as indicated in (2.12).
- R : Resistance of the actuator coil.
- L : Inductance of the actuator coil.

In Table 3-1 the units of the parameters and variables are given, and, if applicable, the values.

Table 3-1: The parameters and variables.

Symbol	Value and units
r	$7 \cdot 10^{-3}$ m
H	$25 \cdot 10^{-3}$ m
Q	Unknown m
M	$9.5 \cdot 10^{-3}$ kg
$C_s$	$1.5 \cdot 10^5$ $\text{kg} \cdot \text{s}^{-2}$
$C_v$	40 $\text{kg} \cdot \text{s}^{-2}$
D	Unknown $\text{kg} \cdot \text{s}^{-1}$
$j_0$	$5.6 \cdot 10^{-8}$ $\text{kg} \cdot \text{m}^2$
$\varepsilon$	$\pi/12$ rad
$h_A$	m
A	3.16 $\text{kg} \cdot \text{m} \cdot \text{s}^{-2} \cdot \text{A}^{-1}$
R	3.5 $\Omega$
L	$1 \cdot 10^{-3}$ H

The damping of the mirror is caused by the mirror rotating in air, and is assumed to be negligible. The value of the damping D has not been measured. This damping is caused by the actuator moving in air, and should also be negligible. The damping is introduced so that if damping is added later the equations still hold.

The mirror is assumed to be symmetrical. Because of this, the inertia matrix is symmetrical as well. All actuators are assumed to be identical.

The local coordinates of  $\underline{a}_i$  can be calculated now r is known. The coordinates can be transformed to global coordinates when the Bryant angles are known, using  $R_B$ .

The global coordinates of  $\underline{\Delta}_i$  can be calculated when  $h_A$  is known. The coordinates can be transformed to local coordinates using  $R_B^T$ . The calculation of  $\underline{a}_i$  and  $\underline{\Delta}_i$  is explained in appendix B.

### 3.1 Mirror dynamics

The dynamics of the mirror will be described using Eulers axiom. Eulers axiom states that the time derivative of the impulse momentum of a rigid body equals the resulting momentum on the body at any time.

Eulers axiom is valid relative to any position. In case of the mirror it is applied relative to the point of rotation of the mirror, in this case the origin of both the local and global frame.

The Bryant angles are used as the kinematic variables. For this reason the angular velocities and angular accelerations have to be known expressed in Bryant angles. The components of

the angular velocities relative to the local frame are described by the vector  $\underline{\omega}$ . For  $\underline{\omega}$  can be found [8]:

$$\underline{\omega} = W_B(\underline{\gamma}) \cdot \underline{\dot{\gamma}} = \begin{bmatrix} \cos(\theta)\cos(\phi) & \sin(\phi) & 0 \\ -\cos(\theta)\sin(\phi) & \cos(\phi) & 0 \\ \sin(\phi) & 0 & 1 \end{bmatrix} \cdot \underline{\dot{\gamma}} \quad (3.1)$$

As a result for the angular acceleration can be found [8]:

$$\underline{\dot{\omega}} = W_B \cdot \underline{\ddot{\gamma}} + \underline{\dot{\omega}}_{BB} \quad (3.2)$$

And by definition [8]:

$$\underline{\dot{\omega}}_{BB} = \begin{bmatrix} \cos(\phi)\dot{\phi}\dot{\theta} - \sin(\phi)\cos(\theta)\dot{\phi}\dot{\psi} - \cos(\phi)\sin(\theta)\dot{\theta}\dot{\psi} \\ -\sin(\phi)\dot{\phi}\dot{\theta} - \cos(\phi)\cos(\theta)\dot{\phi}\dot{\psi} + \sin(\phi)\sin(\theta)\dot{\theta}\dot{\psi} \\ \cos(\theta)\dot{\theta}\dot{\psi} \end{bmatrix} \quad (3.3)$$

Eulers axiom is applied to the mirror in the local frame. Eulers axiom is given by (3.4) . All vectors used in (3.4) have to be in local coordinates.

$$\dot{L}_0 = M_0 \quad (3.4)$$

In (3.4)  $\underline{L}_0$  is the impulse momentum of the mirror relative to the origin, and  $\underline{M}_0$  is the resulting momentum on the mirror.  $\underline{L}_0$  and  $\underline{M}_0$  are given by:

$$L_0 = \int_V \rho r \times \dot{r} dV \quad (3.5)$$

$$M_0 = \sum_i M_i = \sum_i r_i \times E_i \quad (3.6)$$

In (3.5)  $\rho$  is the mass density of the body.

In (3.6)  $\underline{M}_i$  is the momentum on the mirror caused by actuator i.

In the local frame (3.4) can be written as [8]:

$$J_0 \cdot \underline{\dot{\omega}} + \underline{\Omega} \cdot (J_0 \underline{\omega}) = M_0 \quad (3.7)$$

In (3.7) the following holds [8]:

$$\underline{\Omega} = \dot{R}R^T = \begin{bmatrix} 0 & -\omega_3 & \omega_2 \\ \omega_3 & 0 & -\omega_1 \\ -\omega_2 & \omega_1 & 0 \end{bmatrix} \text{ and } J_0 = j_0 \cdot \begin{bmatrix} 1 & 0 & 0 \\ 0 & 1 & 0 \\ 0 & 0 & 1 \end{bmatrix} \quad (3.8)$$

(3.1), (3.2), (3.3) and (3.8) are substituted in (3.7). This results in the nonlinear differential equation for the mirror:

$$\underline{\ddot{\gamma}} = W_B^{-1} J_0^{-1} \{ M_0 - \underline{\Omega} \cdot (J_0 \underline{\omega}) \} - W_B^{-1} \underline{\dot{\omega}}_{BB} \Rightarrow \quad (3.9)$$

$$\begin{bmatrix} \dot{\psi} \\ \ddot{\theta} \\ \ddot{\phi} \end{bmatrix} = j_0^{-1} \begin{bmatrix} \frac{\cos(\phi)}{\cos(\theta)} & -\frac{\sin(\phi)}{\cos(\theta)} & 0 \\ \sin(\phi) & \cos(\phi) & 0 \\ -\cos(\phi)\tan(\theta) & \sin(\phi)\tan(\theta) & 1 \end{bmatrix} M_0 - \begin{bmatrix} \frac{1}{\cos(\theta)}\dot{\theta}\dot{\phi} - \frac{\sin(\theta)}{\cos(\theta)}\dot{\psi}\dot{\theta} \\ -\cos(\theta)\dot{\psi}\dot{\phi} \\ -\frac{\sin(\theta)}{\cos(\theta)}\dot{\theta}\dot{\phi} + \frac{\sin^2(\theta)}{\cos(\theta)}\dot{\psi}\dot{\theta} + \cos(\theta)\dot{\psi}\dot{\theta} \end{bmatrix} \quad (3.10)$$

With (3.10) the dynamics of the mirror are described. The momentum on the mirror are caused by the string forces on the mirror. The momentum will now be described.

The force  $\underline{F}_i$  is exerted on the mirror arm by the string. This force is caused by change in length of the string and the pretensioning. The change in length of the string is defined positive if the string is lengthened, and negative if the string is shortened.

For change in length can be found:

$$\|\underline{a}_i - \underline{A}_i\|_2 - H \quad (3.11)$$

For the magnitude of the string force working on the actuator arm due to length change can be written:

$$-C_s(\|\underline{a}_i - \underline{A}_i\|_2 - H) = -C_s\|\underline{a}_i - \underline{A}_i\|_2 + C_s H \quad (3.12)$$

The pretensioning force magnitude is  $F_0$ . The direction of  $\underline{F}_i$  is  $\underline{a}_i - \underline{A}_i$ . The total string force is the string force due to length change plus the pretensioning force. This means that for  $\underline{F}_i$  can be written:

$$\underline{F}_i = \frac{(\underline{a}_i - \underline{A}_i)}{\|\underline{a}_i - \underline{A}_i\|_2} \left( -C_s\|\underline{a}_i - \underline{A}_i\|_2 + C_s H - F_0 \right) \quad (3.13)$$

This is the force working on the mirror arm. The arm  $\underline{r}_i$  on which  $\underline{F}_i$  works is the same as the vector  $\underline{a}_i$ . Thus for  $\underline{M}_i$  can be found:

$$\underline{M}_i = \underline{a}_i \times \frac{(\underline{a}_i - \underline{A}_i)}{\|\underline{a}_i - \underline{A}_i\|_2} \left( -C_s\|\underline{a}_i - \underline{A}_i\|_2 + C_s H - F_0 \right) \quad (3.14)$$

All vectors in (3.14) must be given in local coordinates.

### 3.2 Actuator dynamics

The actuator coil can only move along the core. Movement along the core is indicated by  $h_{A_i}$ . The direction of each actuator is given by  $\underline{C}_i$  (see appendix B).  $\underline{A}_i$  and  $h_{A_i}$  are related as follows:

$$\underline{A}_i = \underline{O}_i + h_{A_i} \cdot \underline{C}_i \quad (3.15)$$

Only the part of forces working along the actuator core influence the movement of the actuator. The string force on the actuator coil is working in opposite direction of the string force working on the mirror arm. Magnitude of these forces are equal.

As a result the five forces working on the actuator coil are:

1. Inertia force:  $\underline{F}_M$
2. Damping force:  $\underline{F}_D$
3. String force:  $-\underline{F}_i$

4. Spring force:  $E_V$   
 5. Actuator force:  $E_A$

Of these forces only the string force is not working along the core. The part of the string force working along the core is the dot product of the string force and the direction of the core. This force is defined as  $F_S$ . The forces can now be given in magnitude along the core (directed upwards is positive):

$$F_M = -Ms^2 h_A$$

$$F_D = -Dsh_A$$

$$F_S = -E_i \bullet C_i$$

$$F_V = C_V h_A - F_0$$

$$F_A = -AI \text{ or } F_A = \frac{-AU - sA^2 h_A}{R + sL}$$

$F_A$  depends on whether current or voltage control is used.

With (3.13) and with the fact that the sum of the forces is zero the dynamics of the actuator are found in the form of a nonlinear differential equation:

$$-Ms^2 h_{A_i} - Dsh_{A_i} + \frac{(a_i - A_i)}{\|a_i - A_i\|_2} (\|a_i - A_i\|_2 \cdot C_S - HC_S + F_0) \bullet C_i - C_V h_{A_i} - F_0 + F_A \quad (3.16)$$

## 4. Model linearization

In this chapter a linearized model of the system will be derived. In Figure 4.1 the linear and non-linear model are shown. Only one mirror arm is shown. On the left the non-linear system is shown in two positions. In the first position the mirror is not rotated. In the second position

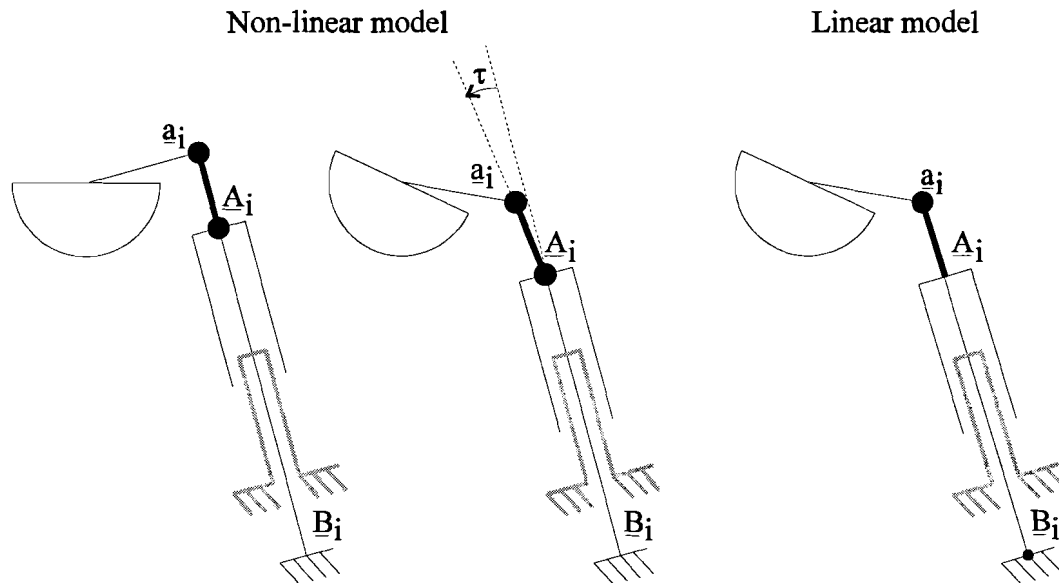


Figure 4.1: Non-linear model and linear model.

the mirror is rotated  $25^\circ$ . As can be seen the coil moves along the actuator. The joints are indicated by dots, the string is drawn by a thick line and the spring is drawn by a thin line. The direction of the string (and therefore the string force) is related to rotation and the mirror and the movement of the actuator along the core.

The string force is not aligned to the actuator core if the mirror is rotated. The angle of the difference in alignment is  $\tau$ , and is a function of the Bryant angles  $\gamma$  and of the actuator position  $h_A$ . The part of the string force along the actuator core is  $-F_i \cos(\tau)$ . In the linearized case this results in the string force being aligned along to actuator core, resulting in the linear model shown on the right.

In the linear model the direction of the spring and of the string are aligned. The direction in the linearized model is therefore only related to the rotation of the mirror which can be described by the Bryant angles.

The part of the string force working sideways on the coil are not zero. This force does not influence the system however because the forces working sideways are assumed to be frictionless.

Lateral movement of the actuator will not be taken into account in the linearization. In the simplified model the string force is working parallel to the other forces working on the actuator. In the real system this is not the case.

The function to be linearized is the function described by (3.10). The product terms in this equation may be linearized separately because only higher order terms will be introduced

when doing so. The total momentum on the mirror  $\underline{M}_0$  is caused by the string forces  $\underline{F}_i$ . The string force  $\underline{F}_i$  is the product of the force direction  $\underline{d}_i$  and the force magnitude  $F_i$ . The momentum caused by one arm is:

$$\underline{M}_i = \underline{r}_i \times \underline{F}_i = \underline{r}_i \times \underline{d}_i \cdot F_i \quad (4.1)$$

The terms in (4.1) may be linearized separately, because only the product operator is used. After finding the linearization of  $\underline{M}_i$ ,  $\underline{M}_0$  linearized can be calculated. This can be substituted in the linearization of (3.10). Higher-order terms may be omitted to result in the linearized model for the mirror.

First  $\underline{F}_i$  will be linearized.

#### 4.1 Linearizing string force magnitude $F_i$

The force magnitude can be found by looking at the forces on one actuator. The actuator is shown in Figure 4.2.

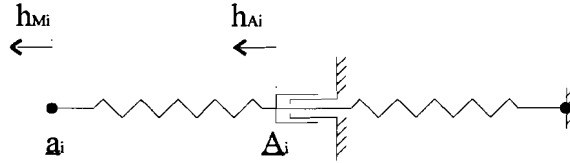


Figure 4.2: The Actuator.

The actuator is attached to the mirror in  $\underline{a}_i$ . The change of length of the string is  $h_{Mi} - h_{Ai}$ .

In this case the nonlinear differential equation (3.15) becomes a linear differential equation:

$$-Ms^2 h_{Ai} - Ds h_{Ai} + C_S(h_{Mi} - h_{Ai}) + F_0 - C_V h_{Ai} - F_0 + F_A \quad (4.2)$$

$F_A$  for current control is:

$$F_A = -AI \quad (4.3)$$

$F_A$  for voltage control is:

$$F_A = \frac{-AU - sA^2 h_A}{R + sL} \quad (4.4)$$

If (4.3) is substituted in (4.2)  $h_{Ai}$  for current control is found:

$$h_{Ai} = \frac{C_S h_{Mi} - AI_i}{Ms^2 + Ds + C_V + C_S} \quad (4.5)$$

If (4.4) is substituted in (4.2)  $h_{Ai}$  for voltage control is found:

$$h_{Ai} = \frac{(R + sL)C_S h_{Mi} - AU_i}{(R + sL)(Ms^2 + Ds + C_V + C_S) + A^2 s} \quad (4.6)$$

The string force magnitude can be given by:

$$F_i = C_S(h_{Ai} - h_{Mi}) - F_0 \quad (4.7)$$

The string force can now be expressed as a function of  $h_{Mi}$ . By substituting (4.5) in (4.7) the string force for current control is found:

$$F_i = \frac{-(C_s Ms^2 + C_s Ds + C_s C_v)h_{Mi} - C_s A I_i}{Ms^2 + Ds + C_s + C_v} - F_0 \quad (4.8)$$

By substituting (4.6) in (4.7) the string force for voltage control is found:

$$F_i = \frac{-C_s h_{Mi} \{(R + sL)(Ms^2 + Ds + C_v) + A^2 s\} - C_s A U_i}{(R + sL)(Ms^2 + Ds + C_s + C_v) + A^2 s} - F_0 \quad (4.9)$$

Now  $h_{Mi}$  needs to be expressed in  $\psi$ .  $h_{Mi}$  will be calculated from the coordinates in the local frame, so by transforming  $\underline{A}_i$  to local coordinates, subtracting the coordinates from  $\underline{a}_i$  in local coordinates and then calculating the change in length. This means that in the local frame the coordinates of  $\underline{a}_i$  are constant and the coordinates of  $\underline{A}_i$  are a function of  $\psi$ . We find:

$$\begin{aligned} h_{Mi} &= \|\underline{a}_i - \underline{B}_i\|_2 - Q = \left\| \begin{bmatrix} x \\ y \\ z \end{bmatrix} - R_B^T \begin{bmatrix} X_G \\ Y_G \\ Z_G \end{bmatrix} \right\|_2 - Q = \left\| \begin{bmatrix} x - X \\ y - Y \\ z - Z \end{bmatrix} \right\|_2 - Q \\ &= \sqrt{(x - X)^2 + (y - Y)^2 + (z - Z)^2} - Q \end{aligned} \quad (4.10)$$

And to linearize  $h_{Mi}$ :

$$\begin{aligned} h_{Mi} &= \left. \frac{\partial \sqrt{(x - X)^2 + (y - Y)^2 + (z - Z)^2}}{\partial \psi} \right|_{\psi=0} \cdot \psi \\ &+ \left. \frac{\partial \sqrt{(x - X)^2 + (y - Y)^2 + (z - Z)^2}}{\partial \theta} \right|_{\theta=0} \cdot \theta \\ &+ \left. \frac{\partial \sqrt{(x - X)^2 + (y - Y)^2 + (z - Z)^2}}{\partial \phi} \right|_{\phi=0} \cdot \phi \end{aligned} \quad (4.11)$$

If (4.11) is applied for  $h_{Mi}$  linearized is found:

$$\begin{aligned} h_{Mi} &= \frac{1}{Q} \left\{ (z - Z_G)Y_G - (y - Y_G)Z_G \right\} \psi \Big|_{\psi=0} \\ &+ \frac{1}{Q} \left\{ (x - X_G)Z_G - (z - Z_G)X_G \right\} \theta \Big|_{\theta=0} \\ &+ \frac{1}{Q} \left\{ (y - Y_G)X_G - (x - X_G)Y_G \right\} \phi \Big|_{\phi=0} \end{aligned} \quad (4.12)$$

The linearized string force can now be calculated using (4.12) and (4.9), and can be applied to the three actuator arms.

## 4.2 Linearizing the string force direction $\underline{d}_i$

The direction of the string force has to be known in local coordinates, because Eulers axiom is applied in the local frame. For the direction can be found:

$$\underline{d}_i = \frac{\underline{a}_i - \underline{B}_i}{\|\underline{a}_i - \underline{B}_i\|_2} = \frac{\begin{bmatrix} x \\ y \\ z \end{bmatrix} - R_B^T \begin{bmatrix} X_G \\ Y_G \\ Z_G \end{bmatrix}}{\left\| \begin{bmatrix} x \\ y \\ z \end{bmatrix} - R_B^T \begin{bmatrix} X_G \\ Y_G \\ Z_G \end{bmatrix} \right\|_2} = \frac{\begin{bmatrix} x - X \\ y - Y \\ z - Z \end{bmatrix}}{\sqrt{(x - X)^2 + (y - Y)^2 + (z - Z)^2}} \quad (4.13)$$

For the linearized direction can be found:

$$\underline{d}_i = \underline{C}_i + \left. \frac{\partial \underline{d}_i}{\partial \psi} \right|_{\psi=0} \cdot \psi + \left. \frac{\partial \underline{d}_i}{\partial \theta} \right|_{\theta=0} \cdot \theta + \left. \frac{\partial \underline{d}_i}{\partial \phi} \right|_{\phi=0} \cdot \phi \quad (4.14)$$

When (4.14) is applied to (4.13) the following is found for the string force direction in local coordinates:

$$\begin{aligned} \underline{d}_i &= \underline{C}_i \\ &+ \left\{ \frac{1}{Q^3} \{(y - Y)Z - (z - Z)Y\} \begin{bmatrix} x - X \\ y - Y \\ z - Z \end{bmatrix} + \frac{1}{Q} \begin{bmatrix} 0 \\ -Z \\ Y \end{bmatrix} \right\}_{\psi=0} \cdot \psi \\ &+ \left\{ \frac{1}{Q^3} \{(z - Z)X - (x - X)Z\} \begin{bmatrix} x - X \\ y - Y \\ z - Z \end{bmatrix} + \frac{1}{Q} \begin{bmatrix} Z \\ 0 \\ -X \end{bmatrix} \right\}_{\theta=0} \cdot \theta \\ &+ \left\{ \frac{1}{Q^3} \{(x - X)Y - (y - Y)X\} \begin{bmatrix} x - X \\ y - Y \\ z - Z \end{bmatrix} + \frac{1}{Q} \begin{bmatrix} -B \\ A \\ 0 \end{bmatrix} \right\}_{\phi=0} \cdot \phi \end{aligned} \quad (4.15)$$

The equations in (4.15) can be applied to the different actuator arms.

## 4.3 The momentum $\underline{M}_1$ on arm 1

In the equilibrium position the following holds for actuator and arm 1:

coordinate	value
x	$r \cos(\epsilon)$
y	0
z	$r \sin(\epsilon)$
X	$r \cos(\epsilon) + Q \sin(\epsilon)$
Y	0
Z	$r \sin(\epsilon) - Q \cos(\epsilon)$



$\underline{C}_i$	$\begin{bmatrix} -\sin(\epsilon) \\ 0 \\ \cos(\epsilon) \end{bmatrix}$
-------------------	--

The linearized momentum can be calculated using the previously derived equations for  $F_i$  and  $\underline{d}_i$ .

The momentum is given by:

$$\underline{M}_i = \underline{r}_i \times \underline{F}_i \quad (4.16)$$

First  $\underline{r}_i \times \underline{d}_i$  will be calculated. The following is found using (4.16):

$$\underline{r}_1 \times \underline{d}_1 = \begin{bmatrix} 0 \\ -r \\ 0 \end{bmatrix} + \begin{bmatrix} -\frac{1}{4}r + \frac{r^2}{Q} \sin^2(\epsilon) & 0 & -r \sin^2(\epsilon) - \frac{r^2}{4Q} \\ 0 & 0 & 0 \\ r \cos^2(\epsilon) - \frac{r^2}{4Q} & 0 & \frac{1}{4}r + \frac{r^2}{Q} \cos^2(\epsilon) \end{bmatrix} \cdot \begin{bmatrix} \Psi \\ \theta \\ \phi \end{bmatrix} \quad (4.17)$$

For  $h_{M1}$  is found using (4.13):

$$h_{M1} = -r\theta \quad (4.18)$$

Equation (4.18) can be used with (4.8) and (4.9) to calculate the string force magnitude  $F_i$ . For current control the string force magnitude becomes:

$$F_1 = \frac{(C_s Ms^2 + C_s Ds + C_s C_v)r\theta - C_s AI_1 - F_0}{Ms^2 + Ds + C_s + C_v} \quad (4.19)$$

With (4.17) the momentum on arm 1 becomes for current control:

$$\underline{M}_1 = \begin{bmatrix} 0 \\ \frac{-(C_s Ms^2 + C_s Ds + C_s C_v)r^2\theta + rCAI_1 + rF_0}{Ms^2 + Ds + C_s + C_v} \\ 0 \end{bmatrix} - F_0 \begin{bmatrix} -\frac{1}{4}r + \frac{r^2}{Q} \sin^2(\epsilon) & 0 & -r \sin^2(\epsilon) - \frac{r^2}{4Q} \\ 0 & 0 & 0 \\ r \cos^2(\epsilon) - \frac{r^2}{4Q} & 0 & \frac{1}{4}r + \frac{r^2}{Q} \cos^2(\epsilon) \end{bmatrix} \cdot \begin{bmatrix} \Psi \\ \theta \\ \phi \end{bmatrix} \quad (4.20)$$

For voltage control the string force magnitude becomes:

$$F_1 = \frac{r\theta C_s \{ (R + sL)(Ms^2 + Ds + C_v) + A^2 s \} - C_s AU_1 - F_0}{(R + sL)(Ms^2 + Ds + C_s + C_v) + A^2 s} \quad (4.21)$$

With (4.17) the momentum on arm 1 becomes for voltage control:

$$\underline{M}_1 = \begin{bmatrix} 0 \\ -r^2\theta C_s \left\{ (R+sL)(Ms^2 + Ds + C_v) + A^2s \right\} + rC_s AU_i \\ (R+sL)(Ms^2 + Ds + C_s + C_v) + A^2s \\ 0 \end{bmatrix} + rF_0$$

$$-F_0 \begin{bmatrix} -\frac{1}{4}r + \frac{r^2}{Q}\sin^2(\epsilon) & 0 & -r\sin^2(\epsilon) - \frac{r^2}{4Q} \\ 0 & 0 & 0 \\ r\cos^2(\epsilon) - \frac{r^2}{4Q} & 0 & \frac{1}{4}r + \frac{r^2}{Q}\cos^2(\epsilon) \end{bmatrix} \cdot \begin{bmatrix} \psi \\ \theta \\ \phi \end{bmatrix} \quad (4.22)$$

#### 4.4 The momentum $\underline{M}_2$ on arm 2

In the equilibrium position the following holds for actuator and arm 2:

coordinate	value
x	$-\frac{1}{2}r\cos(\epsilon)$
y	$\frac{1}{2}\sqrt{3}r\cos(\epsilon)$
z	$r\sin(\epsilon)$
X	$-\frac{1}{2}(r\cos(\epsilon)+Q\sin(\epsilon))$
Y	$\frac{1}{2}\sqrt{3}(r\cos(\epsilon)+Q\sin(\epsilon))$
Z	$r\sin(\epsilon)-Q\cos(\epsilon)$
$\underline{C}_i$	$\begin{bmatrix} \frac{1}{2}\sin(\epsilon) \\ -\frac{1}{2}\sqrt{3}\sin(\epsilon) \\ \cos(\epsilon) \end{bmatrix}$

The linearized momentum can be calculated using the previously derived equations for  $F_i$  and  $\underline{d}_i$ .

First  $\underline{r}_i \times \underline{d}_i$  will be calculated. The following is found using (4.15):

$$\underline{r}_2 \times \underline{d}_2 = \begin{bmatrix} \frac{1}{2}\sqrt{3}r \\ \frac{1}{2}r \\ 0 \end{bmatrix}$$

$$+ \begin{bmatrix} -\frac{1}{16}r + \frac{r^2}{4Q}\sin^2(\epsilon) & -\sqrt{3}\frac{r^2}{4Q}\sin^2(\epsilon) + \frac{1}{16}\sqrt{3}r & \frac{1}{2}r\sin^2(\epsilon) + \frac{r^2}{8Q} \\ \frac{1}{16}\sqrt{3}r - \sqrt{3}\frac{r^2}{4Q}\sin^2(\epsilon) & -\frac{3}{16}r + \frac{3r^2}{4Q}\sin^2(\epsilon) & -\frac{1}{2}\sqrt{3}r\sin^2(\epsilon) - \sqrt{3}\frac{r^2}{8Q} \\ -\frac{1}{2}r\cos^2(\epsilon) + \frac{r^2}{8Q} & \frac{1}{2}\sqrt{3}r\cos^2(\epsilon) - \sqrt{3}\frac{r^2}{8Q} & \frac{1}{4}r + \frac{r^2}{Q}\cos^2(\epsilon) \end{bmatrix} \cdot \begin{bmatrix} \psi \\ \theta \\ \phi \end{bmatrix} \quad (4.23)$$

For  $h_{M2}$  is found using (4.12):

$$h_{M2} = \frac{1}{2}\sqrt{3}r\psi + \frac{1}{2}r\theta \quad (4.24)$$

For current control the string force magnitude becomes:

$$F_2 = \frac{-(C_S Ms^2 + C_S Ds + C_S C_V)(\frac{1}{2}\sqrt{3}r\psi + \frac{1}{2}r\theta) - C_S AI_2}{Ms^2 + Ds + C_S + C_V} - F_0 \quad (4.25)$$

With (4.17) the momentum on arm 2 becomes for current control:

$$\underline{M}_2 = \begin{bmatrix} \frac{-(C_S Ms^2 + C_S Ds + C_S C_V)(\frac{3}{4}r^2\psi + \frac{1}{4}\sqrt{3}r^2\theta) - \frac{1}{2}\sqrt{3}rC_S AI_2}{Ms^2 + Ds + C_S + C_V} - \frac{1}{2}\sqrt{3}rF_0 \\ \frac{-(C_S Ms^2 + C_S Ds + C_S C_V)(\frac{1}{4}\sqrt{3}r^2\psi + \frac{1}{4}r^2\theta) - \frac{1}{2}rC_S AI_2}{Ms^2 + Ds + C_S + C_V} - \frac{1}{2}rF_0 \\ 0 \end{bmatrix} \quad (4.26)$$

$$-F_0 \begin{bmatrix} -\frac{1}{16}r + \frac{r^2}{4Q} \sin^2(\epsilon) & -\sqrt{3} \frac{r^2}{4Q} \sin^2(\epsilon) + \frac{1}{16}\sqrt{3}r & \frac{1}{2}r \sin^2(\epsilon) + \frac{r^2}{8Q} \\ \frac{1}{16}\sqrt{3}r - \sqrt{3} \frac{r^2}{4Q} \sin^2(\epsilon) & -\frac{3}{16}r + \frac{3r^2}{4Q} \sin^2(\epsilon) & -\frac{1}{2}\sqrt{3}r \sin^2(\epsilon) - \sqrt{3} \frac{r^2}{8Q} \\ -\frac{1}{2}r \cos^2(\epsilon) + \frac{r^2}{8Q} & \frac{1}{2}\sqrt{3}r \cos^2(\epsilon) - \sqrt{3} \frac{r^2}{8Q} & \frac{1}{4}r + \frac{r^2}{Q} \cos^2(\epsilon) \end{bmatrix} \cdot \begin{bmatrix} \psi \\ \theta \\ \phi \end{bmatrix}$$

For voltage control the string force magnitude becomes:

$$F_2 = \frac{-(\frac{1}{2}\sqrt{3}r\psi + \frac{1}{2}r\theta C_S) \left\{ (R + sL)(Ms^2 + Ds + C_V) + A^2s \right\} - C_S AU_2}{(R + sL)(Ms^2 + Ds + C_S + C_V) + A^2s} - F_0 \quad (4.27)$$

With (4.17) the momentum on arm 3 becomes for voltage control:

$$\underline{M}_2 = \begin{bmatrix} \frac{-(\frac{3}{4}r^2\psi + \frac{1}{4}\sqrt{3}r^2\theta)C_S \left\{ (R + sL)(Ms^2 + Ds + C_V) + A^2s \right\} - \frac{1}{2}\sqrt{3}rC_S AU_2}{(R + sL)(Ms^2 + Ds + C_S + C_V) + A^2s} - \frac{1}{2}\sqrt{3}rF_0 \\ \frac{-(\frac{1}{4}\sqrt{3}r^2\psi + \frac{1}{4}r^2\theta)C_S \left\{ (R + sL)(Ms^2 + Ds + C_V) + A^2s \right\} - \frac{1}{2}rC_S AU_2}{(R + sL)(Ms^2 + Ds + C_S + C_V) + A^2s} - \frac{1}{2}rF_0 \\ 0 \end{bmatrix} \quad (4.28)$$

$$-F_0 \begin{bmatrix} -\frac{1}{16}r + \frac{r^2}{4Q} \sin^2(\epsilon) & -\sqrt{3} \frac{r^2}{4Q} \sin^2(\epsilon) + \frac{1}{16}\sqrt{3}r & \frac{1}{2}r \sin^2(\epsilon) + \frac{r^2}{8Q} \\ \frac{1}{16}\sqrt{3}r - \sqrt{3} \frac{r^2}{4Q} \sin^2(\epsilon) & -\frac{3}{16}r + \frac{3r^2}{4Q} \sin^2(\epsilon) & -\frac{1}{2}\sqrt{3}r \sin^2(\epsilon) - \sqrt{3} \frac{r^2}{8Q} \\ -\frac{1}{2}r \cos^2(\epsilon) + \frac{r^2}{8Q} & \frac{1}{2}\sqrt{3}r \cos^2(\epsilon) - \sqrt{3} \frac{r^2}{8Q} & \frac{1}{4}r + \frac{r^2}{Q} \cos^2(\epsilon) \end{bmatrix} \cdot \begin{bmatrix} \psi \\ \theta \\ \phi \end{bmatrix}$$

## 4.5 The momentum $\underline{M}_3$ on arm 3

In the equilibrium position the following holds for actuator and arm 3:

coordinate	value
x	$-\frac{1}{2}r\cos(\epsilon)$
y	$-\frac{1}{2}\sqrt{3}r\cos(\epsilon)$
z	$r\sin(\epsilon)$
X	$-\frac{1}{2}(r\cos(\epsilon)+Q\sin(\epsilon))$
Y	$-\frac{1}{2}\sqrt{3}(r\cos(\epsilon)+Q\sin(\epsilon))$
Z	$r\sin(\epsilon)-Q\cos(\epsilon)$
$\underline{C}_i$	$\begin{bmatrix} \frac{1}{2}\sin(\epsilon) \\ \frac{1}{2}\sqrt{3}\sin(\epsilon) \\ \cos(\epsilon) \end{bmatrix}$

The linearized momentum can be calculated using the previously derived equations for  $F_i$  and  $\underline{d}_i$ .

First  $\underline{r}_i \times \underline{d}_i$  will be calculated. The following is found using (4.15):

$$\underline{r}_3 \times \underline{d}_3 = \begin{bmatrix} -\frac{1}{2}\sqrt{3}r \\ \frac{1}{2}r \\ 0 \end{bmatrix} + \begin{bmatrix} -\frac{1}{16}r + \frac{r^2}{4Q}\sin^2(\epsilon) & +\sqrt{3}\frac{r^2}{4Q}\sin^2(\epsilon) - \frac{1}{16}\sqrt{3}r & \frac{1}{2}r\sin^2(\epsilon) + \frac{r^2}{8Q} \\ -\frac{1}{16}\sqrt{3}r + \sqrt{3}\frac{r^2}{4Q}\sin^2(\epsilon) & -\frac{3}{16}r + \frac{3r^2}{4Q}\sin^2(\epsilon) & \frac{1}{2}\sqrt{3}r\sin^2(\epsilon) + \sqrt{3}\frac{r^2}{8Q} \\ -\frac{1}{2}r\cos^2(\epsilon) + \frac{r^2}{8Q} & -\frac{1}{2}\sqrt{3}r\cos^2(\epsilon) + \sqrt{3}\frac{r^2}{8Q} & \frac{1}{4}r + \frac{r^2}{Q}\cos^2(\epsilon) \end{bmatrix} \cdot \begin{bmatrix} \psi \\ \theta \\ \phi \end{bmatrix} \quad (4.29)$$

For  $h_{M3}$  is found using (4.12):

$$h_{M3} = -\frac{1}{2}\sqrt{3}r\psi + \frac{1}{2}r\theta \quad (4.30)$$

For current control the string force magnitude becomes:

$$F_3 = \frac{-(C_s Ms^2 + C_s Ds + C_s C_v)(-\frac{1}{2}\sqrt{3}r\psi + \frac{1}{2}r\theta) - C_s AI_3}{Ms^2 + Ds + C_s + C_v} - F_0 \quad (4.31)$$

With (4.17) the momentum on arm 3 becomes for current control:

$$\underline{M}_3 = \begin{bmatrix} \frac{-(C_S Ms^2 + C_S Ds + C_S C_V)(\frac{3}{4}r^2\psi - \frac{1}{4}\sqrt{3}r^2\theta) + \frac{1}{2}\sqrt{3}rC_S AI_3 + \frac{1}{2}\sqrt{3}rF_0}{Ms^2 + Ds + C_S + C_V} \\ \frac{-(C_S Ms^2 + C_S Ds + C_S C_V)(-\frac{1}{4}\sqrt{3}r^2\psi + \frac{1}{4}r^2\theta) - \frac{1}{2}rC_S AI_3 - \frac{1}{2}rF_0}{Ms^2 + Ds + C_S + C_V} \\ 0 \end{bmatrix} \quad (4.32)$$

$$-F_0 \begin{bmatrix} -\frac{1}{16}r + \frac{r^2}{4Q}\sin^2(\epsilon) & +\sqrt{3}\frac{r^2}{4Q}\sin^2(\epsilon) - \frac{1}{16}\sqrt{3}r & \frac{1}{2}r\sin^2(\epsilon) + \frac{r^2}{8Q} \\ -\frac{1}{16}\sqrt{3}r + \sqrt{3}\frac{r^2}{4Q}\sin^2(\epsilon) & -\frac{3}{16}r + \frac{3r^2}{4Q}\sin^2(\epsilon) & \frac{1}{2}\sqrt{3}r\sin^2(\epsilon) + \sqrt{3}\frac{r^2}{8Q} \\ -\frac{1}{2}r\cos^2(\epsilon) + \frac{r^2}{8Q} & -\frac{1}{2}\sqrt{3}r\cos^2(\epsilon) + \sqrt{3}\frac{r^2}{8Q} & \frac{1}{4}r + \frac{r^2}{Q}\cos^2(\epsilon) \end{bmatrix} \cdot \begin{bmatrix} \psi \\ \theta \\ \phi \end{bmatrix}$$

For voltage control the string force magnitude becomes:

$$F_3 = \frac{-(-\frac{1}{2}\sqrt{3}r\psi + \frac{1}{2}r\theta C_S) \left\{ (R + sL)(Ms^2 + Ds + C_V) + A^2s \right\} - C_S AU_3}{(R + sL)(Ms^2 + Ds + C_S + C_V) + A^2s} - F_0 \quad (4.33)$$

With (4.17) the momentum on arm 3 becomes for voltage control:

$$\underline{M}_3 = \begin{bmatrix} \frac{-(\frac{3}{4}r^2\psi - \frac{1}{4}\sqrt{3}r^2\theta)C_S \left\{ (R + sL)(Ms^2 + Ds + C_V) + A^2s \right\} + \frac{1}{2}\sqrt{3}rC_S AU_3 + \frac{1}{2}\sqrt{3}rF_0}{(R + sL)(Ms^2 + Ds + C_S + C_V) + A^2s} \\ \frac{-(-\frac{1}{4}\sqrt{3}r^2\psi + \frac{1}{4}r^2\theta)C_S \left\{ (R + sL)(Ms^2 + Ds + C_V) + A^2s \right\} - \frac{1}{2}rC_S AU_3 - \frac{1}{2}rF_0}{(R + sL)(Ms^2 + Ds + C_S + C_V) + A^2s} \\ 0 \end{bmatrix} \quad (4.34)$$

$$-F_0 \begin{bmatrix} -\frac{1}{16}r + \frac{r^2}{4Q}\sin^2(\epsilon) & +\sqrt{3}\frac{r^2}{4Q}\sin^2(\epsilon) - \frac{1}{16}\sqrt{3}r & \frac{1}{2}r\sin^2(\epsilon) + \frac{r^2}{8Q} \\ -\frac{1}{16}\sqrt{3}r + \sqrt{3}\frac{r^2}{4Q}\sin^2(\epsilon) & -\frac{3}{16}r + \frac{3r^2}{4Q}\sin^2(\epsilon) & \frac{1}{2}\sqrt{3}r\sin^2(\epsilon) + \sqrt{3}\frac{r^2}{8Q} \\ -\frac{1}{2}r\cos^2(\epsilon) + \frac{r^2}{8Q} & -\frac{1}{2}\sqrt{3}r\cos^2(\epsilon) + \sqrt{3}\frac{r^2}{8Q} & \frac{1}{4}r + \frac{r^2}{Q}\cos^2(\epsilon) \end{bmatrix} \cdot \begin{bmatrix} \psi \\ \theta \\ \phi \end{bmatrix}$$

## 4.6 The total momentum $\underline{M}_0$ on the mirror

The total momentum on the mirror can be calculated by simply adding the momentum on the arms. This way for current control can be found:

$$\begin{aligned}
\mathbf{M}_0 &= \sum_{i=1}^3 \mathbf{M}_i \Rightarrow \\
\mathbf{M}_0 &= \begin{bmatrix} \frac{-(C_s Ms^2 + C_s Ds + C_s C_v) \left( \frac{3}{2} r^2 \psi \right) + \frac{1}{2} \sqrt{3} r C_s A (I_3 - I_2)}{Ms^2 + Ds + C_v + C_s} \\ \frac{-(C_s Ms^2 + C_s Ds + C_s C_v) \left( \frac{3}{2} r^2 \theta \right) + r C_s A (I_1 - \frac{1}{2} I_2 - \frac{1}{2} I_3)}{Ms^2 + Ds + C_v + C_s} \\ 0 \end{bmatrix} \\
& -F_0 \begin{bmatrix} \psi \left\{ -\frac{3}{8} r + \frac{3r^2}{2Q} \sin^2(\epsilon) \right\} \\ \theta \left\{ -\frac{3}{8} r + \frac{3r^2}{2Q} \sin^2(\epsilon) \right\} \\ \phi \left\{ \frac{3}{4} r + \frac{3r^2}{Q} \cos^2(\epsilon) \right\} \end{bmatrix} \tag{4.35}
\end{aligned}$$

For voltage control:

$$\begin{aligned}
\mathbf{M}_0 &= \begin{bmatrix} \frac{-\frac{3}{2} r^2 \psi C_s \{ (R + sL)(Ms^2 + Ds + C_v) + A^2 s \} + \frac{1}{2} \sqrt{3} r C_s A (U_3 - U_2)}{(R + sL)(Ms^2 + Ds + C_v + C_s) + A^2 s} \\ \frac{-\frac{3}{2} r^2 \theta C_s \{ (R + sL)(Ms^2 + Ds + C_v) + A^2 s \} + r C_s A (U_1 - \frac{1}{2} U_2 - \frac{1}{2} U_3)}{(R + sL)(Ms^2 + Ds + C_v + C_s) + A^2 s} \\ 0 \end{bmatrix} \\
& -F_0 \begin{bmatrix} \psi \left\{ -\frac{3}{8} r + \frac{3r^2}{2Q} \sin^2(\epsilon) \right\} \\ \theta \left\{ -\frac{3}{8} r + \frac{3r^2}{2Q} \sin^2(\epsilon) \right\} \\ \phi \left\{ \frac{3}{4} r + \frac{3r^2}{Q} \cos^2(\epsilon) \right\} \end{bmatrix} \tag{4.36}
\end{aligned}$$

## 4.7 The linear system description

The equations (4.35) and (4.36) must be substituted into (3.10) to get the equations that describe the system. A linear system description needs to be found. The equations (4.35) and (4.36) only contain first-order terms. This means that (3.10) may be reduced to a zero-order equation, because higher order terms will be discarded after substitution. Leaving only zero order terms (3.10) becomes:

$$\begin{bmatrix} \ddot{\psi} \\ \ddot{\theta} \\ \ddot{\phi} \end{bmatrix} = j_0^{-1} \begin{bmatrix} 1 & 0 & 0 \\ 0 & 1 & 0 \\ 0 & 0 & 1 \end{bmatrix} \mathbf{M}_0 \tag{4.37}$$

If (4.35) and (4.36) are substituted in (4.37) the linear system description is found for current and voltage control. The linear differential equations become for current control:

$$\psi = \frac{\frac{1}{2}\sqrt{3}rC_s A(I_3 - I_2)}{N_i} \quad (4.38)$$

$$\theta = \frac{rC_s A(I_1 - \frac{1}{2}I_2 - \frac{1}{2}I_3)}{N_i} \quad (4.39)$$

$$\phi = 0 \quad (4.40)$$

The denominator in (4.38) and (4.39) is:

$$\begin{aligned} N_i = & j_0 Ms^4 \\ & + j_0 Ds^3 \\ & + \{j_0(C_v + C_s) + \frac{3}{2}r^2 MC_s + MF_0V\}s^2 \\ & + (\frac{3}{2}r^2 DC_s + DF_0V)s \\ & + (C_v + C_s)F_0V + \frac{3}{2}r^2 C_v C_s \end{aligned} \quad (4.41)$$

V is given by:

$$V = -\frac{3}{2}r \sin(\epsilon) \cos(\epsilon) + \frac{3r^2}{2H} \sin^2(\epsilon) = \frac{-3}{8}r + \frac{3r^2}{2H} \sin^2(\epsilon) \quad (4.42)$$

For voltage control the equations become:

$$\psi = \frac{\frac{1}{2}\sqrt{3}rC_s A(U_3 - U_2)}{N_u} \quad (4.43)$$

$$\theta = \frac{rC_s A(U_1 - \frac{1}{2}U_2 - \frac{1}{2}U_3)}{N_u} \quad (4.44)$$

$$\phi = 0 \quad (4.45)$$

For the denominator  $N_u$  in (4.43) and (4.44) can be written:

$$\begin{aligned} N_u = & j_0 MLs^5 \\ & + j_0 (DL + MR)s^4 \\ & + [j_0 \{DR + L(C_s + C_v) + A^2\} + F_0VML + \frac{3}{2}r^2 C_s ML]s^3 \\ & + \{j_0 R(C_s + C_v) + F_0V(DL + MR) + \frac{3}{2}r^2 C_s (MR + DL)\}s^2 \\ & + [F_0V \{DR + L(C_v + C_s) + A^2\} + \frac{3}{2}r^2 C_s (RD + C_v L + A^2)]s \\ & + F_0VR(C_v + C_s) + \frac{3}{2}r^2 RC_v C_s \end{aligned} \quad (4.46)$$

For current control the system is of 8th order. This can be understood as follows:

The system is linearly described by two rotations, one around  $\psi$ , and one around  $\theta$ . The 3 actuators together have order 6. Because of the linearization the actuators become of order 2

for every rotation. The mirror is of order 2 for every rotation. Because the system is linearly described by two rotations, the result is 2 systems of order 4. The total order is therefore 8. The transfer functions for the angles  $\alpha$  and  $\beta$  are the same as for  $\psi$  and  $\theta$ . For  $\alpha$  this can easily be seen since  $\alpha=\psi$ . If (2.7) is linearized it is easily found that  $\beta=\theta$ .

The transfer functions can be rewritten to form SISO functions.  $I_\psi$  and  $I_\theta$  are defined as:

$$\begin{aligned} I_\psi &= I_3 - I_2 \\ I_\theta &= I_1 - \frac{1}{2}I_2 - \frac{1}{2}I_3 \end{aligned} \quad (4.47)$$

and therefore:

$$\begin{bmatrix} I_\psi \\ I_\theta \end{bmatrix} = \begin{bmatrix} 0 & -1 & 1 \\ 1 & -\frac{1}{2} & -\frac{1}{2} \end{bmatrix} \cdot \begin{bmatrix} I_1 \\ I_2 \\ I_3 \end{bmatrix} \text{ and } \begin{bmatrix} I_1 \\ I_2 \\ I_3 \end{bmatrix} = \begin{bmatrix} 0 & \frac{2}{3} \\ -\frac{1}{2} & -\frac{1}{3} \\ \frac{1}{2} & -\frac{1}{3} \end{bmatrix} \cdot \begin{bmatrix} I_\psi \\ I_\theta \end{bmatrix} \quad (4.48)$$

Using (4.49) in (4.39) and (4.40) results in two SISO functions:

$$\psi = \frac{\frac{1}{2}\sqrt{3}rC_s AI_\psi}{N_i} \quad (4.49)$$

$$\theta = \frac{rC_s AI_\theta}{N_i} \quad (4.50)$$

In case of voltage control, the system is of 10<sup>th</sup> order. Here the mirror is again is a 2<sup>nd</sup> order system for every rotation. The 3 actuators together are of order 9. Because of the linearization the actuators become of order 3 for every rotation. The result is 2 systems of order 5 for every rotation. In the linear case the only rotations are around  $\psi$  and  $\theta$ . The result is a 10<sup>th</sup> order system.

Similar to the current controlled system for the voltage controlled system can be defined:

$$\begin{bmatrix} U_\psi \\ U_\theta \end{bmatrix} = \begin{bmatrix} 0 & -1 & 1 \\ 1 & -\frac{1}{2} & -\frac{1}{2} \end{bmatrix} \cdot \begin{bmatrix} U_1 \\ U_2 \\ U_3 \end{bmatrix} \text{ and } \begin{bmatrix} U_1 \\ U_2 \\ U_3 \end{bmatrix} = \begin{bmatrix} 0 & \frac{2}{3} \\ -\frac{1}{2} & -\frac{1}{3} \\ \frac{1}{2} & -\frac{1}{3} \end{bmatrix} \cdot \begin{bmatrix} U_\psi \\ U_\theta \end{bmatrix} \quad (4.51)$$

Using (4.52) in (4.44) and (4.45) results in two SISO systems:

$$\psi = \frac{\frac{1}{2}\sqrt{3}rC_s AU_\psi}{N_u} \quad (4.52)$$

$$\theta = \frac{rC_s AU_\theta}{N_u} \quad (4.53)$$



## 4.8 Linear characteristics

From the transfer functions it can be seen that  $\phi$  cannot be controlled for current and voltage control. The sensor on the mirror measure sensor angles  $\alpha$  and  $\beta$ . From these variables  $\phi$  cannot be calculated. In the linear case it is therefore impossible to control  $\phi$ .

### 4.8.1 Pole placement

From the transfer functions it can be seen that for both current and voltage control the linear system has no zeros. When current control is used, the system has 4 poles. When voltage control is used the system has 5 poles. It can also be seen that  $F_0$  influences transfer functions. The equilibrium length of the spring and the string together is  $Q$ .  $Q$  is not known, but still influences the transfer function.  $F_0$  is chosen zero. In that case  $Q$  and  $F_0$  do not influence the transfer functions. If  $F_0$  is taken to be zero the transfer functions become:

$$\Psi = \frac{5.4013 \cdot 10^{12} \cdot I_\psi}{s^4 + 2.1267 \cdot 10^8 s^2 + 8.2895 \cdot 10^{11}} \quad (4.54)$$

$$\theta = \frac{6.2368 \cdot 10^{12} \cdot I_\theta}{s^4 + 2.1267 \cdot 10^8 s^2 + 8.2895 \cdot 10^{11}}$$

for current control and

$$\Psi = \frac{5.4013 \cdot 10^{15} \cdot U_\psi}{s^5 + 3.5 \cdot 10^3 s^4 + 2.1372 \cdot 10^8 s^3 + 7.4434 \cdot 10^{11} s^2 + 2.0777 \cdot 10^{14} s + 2.9013 \cdot 10^{15}} \quad (4.55)$$

$$\theta = \frac{6.2368 \cdot 10^{15} \cdot U_\theta}{s^5 + 3.5 \cdot 10^3 s^4 + 2.1372 \cdot 10^8 s^3 + 7.4434 \cdot 10^{11} s^2 + 2.0777 \cdot 10^{14} s + 2.9013 \cdot 10^{15}}$$

for voltage control.

From these functions the poles can be calculated if  $F_0$  is zero. The poles for current control are two imaginary conjugate pole pairs. The poles are at:

- $1.4583 \cdot 10^4 j$
- $-1.4583 \cdot 10^4 j$
- $6.2433 \cdot 10^1 j$
- $-6.2433 \cdot 10^1 j$

The resulting resonance frequencies are at 2.32 kHz for the first pole pair, and 9.93 Hz for the second pole pair.

When voltage control is used, there are three real negative poles and one complex pole pair.

The poles are at:

- $-6.1233 \cdot 10^1 + 1.4586 \cdot 10^4 j$
- $-6.1233 \cdot 10^1 - 1.4586 \cdot 10^4 j$
- $-3.1944 \cdot 10^3$
- $-2.8966 \cdot 10^2$
- $-1.4739 \cdot 10^1$

The resonance frequency of the complex pole pair is at 2.32 kHz. This is a slightly damped oscillation: the damping ratio is  $4.20 \cdot 10^{-5}$ .

The pole at  $-1.4739 \cdot 10^1$  determines the largest time constant. The largest time constant of the linear system is 0.43 seconds.

If the pretensioning force is increased, the pole placement changes. Pole placement as a function of the pretensioning force is calculated using Matlab. How the poles change can be seen in Figure 4.3, note that the plot is not correctly scaled. The crosses indicate the poles when  $F_0$  is zero. The arrows indicate the direction of the pole movement when  $F_0$  increases. In case of current control poles move towards to origin.

Increasing the pretensioning using voltage control causes the slowest pole to move to the right. From the transfer functions it can be concluded that the system can become unstable

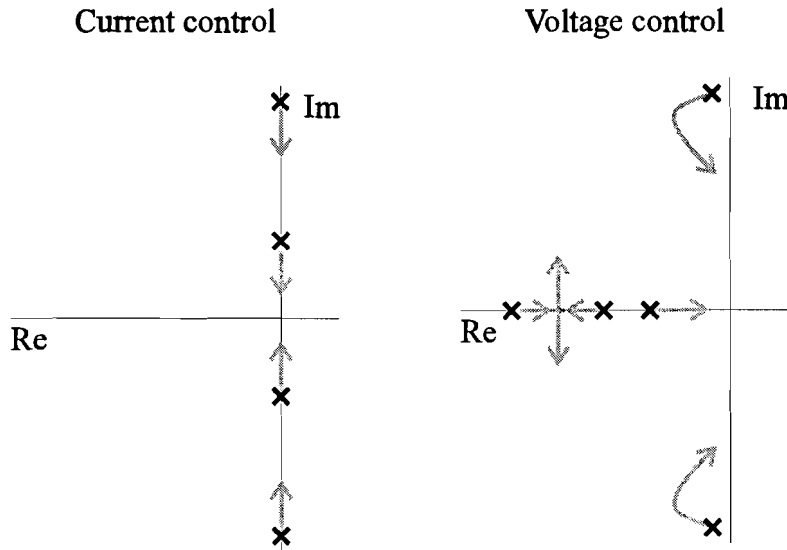


Figure 4.3: Pole movement as a function of  $F_0$ .

when the pretensioning force is increased. Physically this is not possible however. The pretensioning force cannot be bigger than the length of the string and the spring together times the spring constant of the spring:

$$F_0 < Q \cdot C_v \tag{4.56}$$

Under this condition the transfer function is never unstable.

### 4.8.2 Step responses

From the transfer functions the step responses of the linear system can be calculated. For this purpose Matlab is used. A unity step was not applied since the rotation of the mirror is limited, and a unity step would cause the mirror to rotate beyond that limit. The step amplitudes for current and voltage control are shown in Table 4-1.

Table 4-1: Step amplitudes.

Current control	Voltage control
$I_\psi = 50\text{mA}$	$U_\psi = 0.15\text{ V}$
$I_\theta = 50\text{mA}$	$U_\theta = 0.15\text{ V}$

Only the gains of the transfer functions are different. For this reason only the step responses of  $\psi$  will be shown. (The characteristics for  $\psi$  and  $\theta$  are the same.)

The step responses are shown in Figure 4.4.

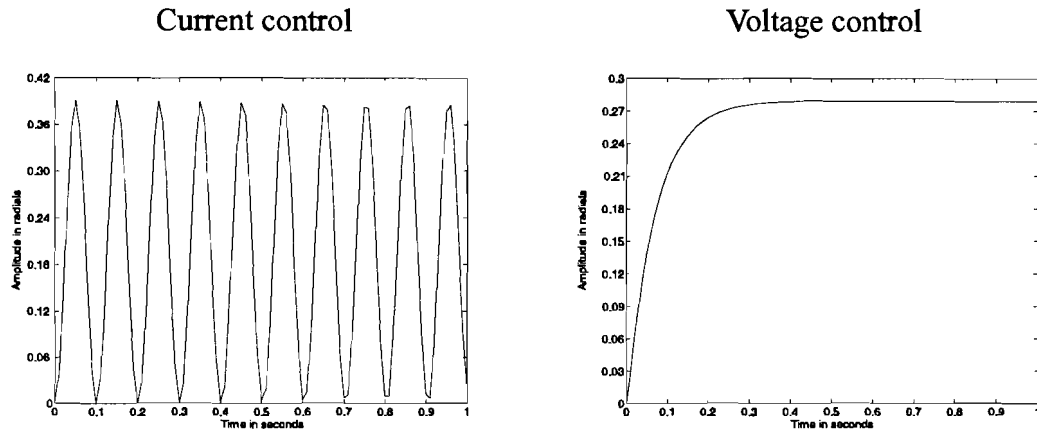


Figure 4.4: Linear step responses.

From the step response using current control it can be found that the resonance frequencies for both  $\psi$  and  $\theta$  are about 9.9 Hz, as expected from the pole placement.

When voltage control is used, the step response shows that the final value is reached after about 0.5 seconds.

#### 4.8.3 Bode plots of the linear model

In this section the Bode plots will be given. Since only the DC gain is different for the  $\psi$  and  $\theta$ , only the plots will be given for  $\psi$ . The characteristics for both plots are the same. The plots are shown in Figure 4.5.

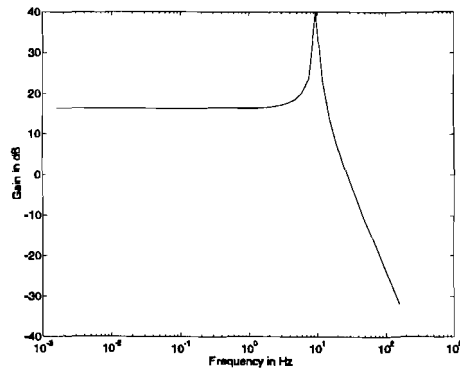
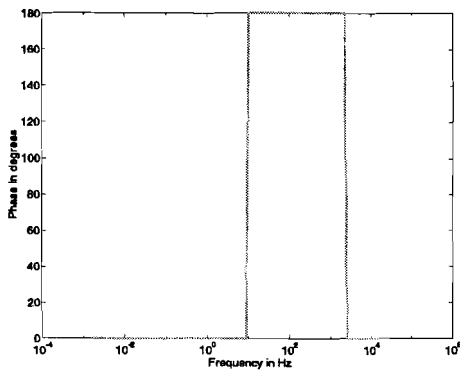
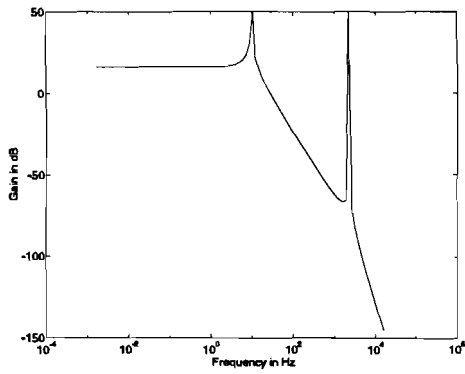
For both current and voltage control the amplitude and phase plots are shown. Also the Bode plot over a limited frequency range is shown. The resonance frequencies show up clearly in the Bode plots.

From the Bode plots it can be seen that the -40 dB point from the DC-gain are at about 100 Hz. This is the point at which the amplitudes have decreased a factor 100 from the DC-gain.

The -3 dB point from the DC-gain will be called the cutoff frequency. The cutoff frequency is decreased when  $F_0$  is increased. This can be seen in Figure 4.3. The slowest pole moves towards the origin if  $F_0$  is increased. Measurements were done on the real system, showing that the cutoff frequency is at 5 Hz using voltage control. This value cannot be achieved in the simulation, the highest value for the cutoff frequency is 2.35 Hz. The reason for this might be that the system parameters used in the simulation differ from the real values. The real system might be given a faster response by decreasing the  $F_0$ .

The simulation will be used to identify the system. Therefore  $F_0$  will be given the value zero, to resemble the response of the real system the most. Also the unknown length of  $Q$  has no influence in this case. The system behaviour in this case is as shown in Figure 4.4.

Current control



Voltage control

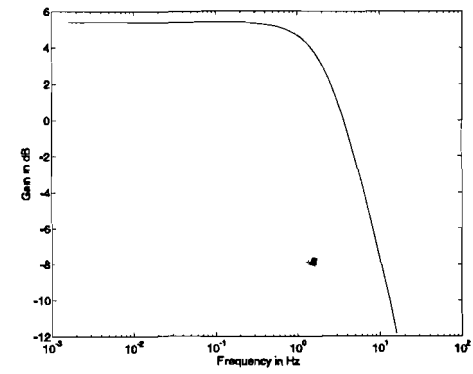
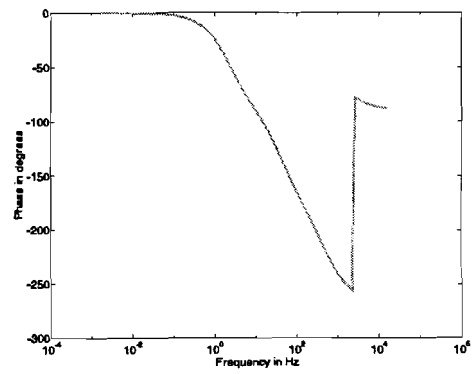
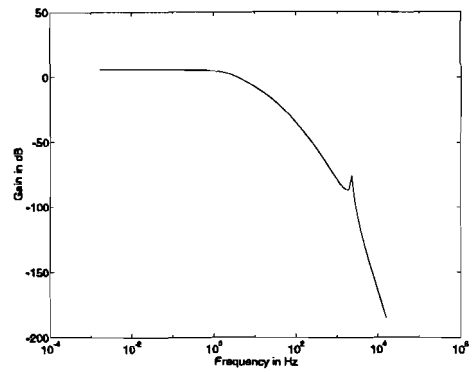


Figure 4.5: Bode plots of the linear model.

## 5. System simulation

The nonlinear differential equations (3.10) and (3.15) are used to build a simulation of the laser deflecting system. The simulation is programmed using Mathworks' Simulink [7], and is not based on the simplified model used in the linearization, but based on the actual model. In Figure 5.1 a block diagram is shown of how the equations are implemented in the simulation.

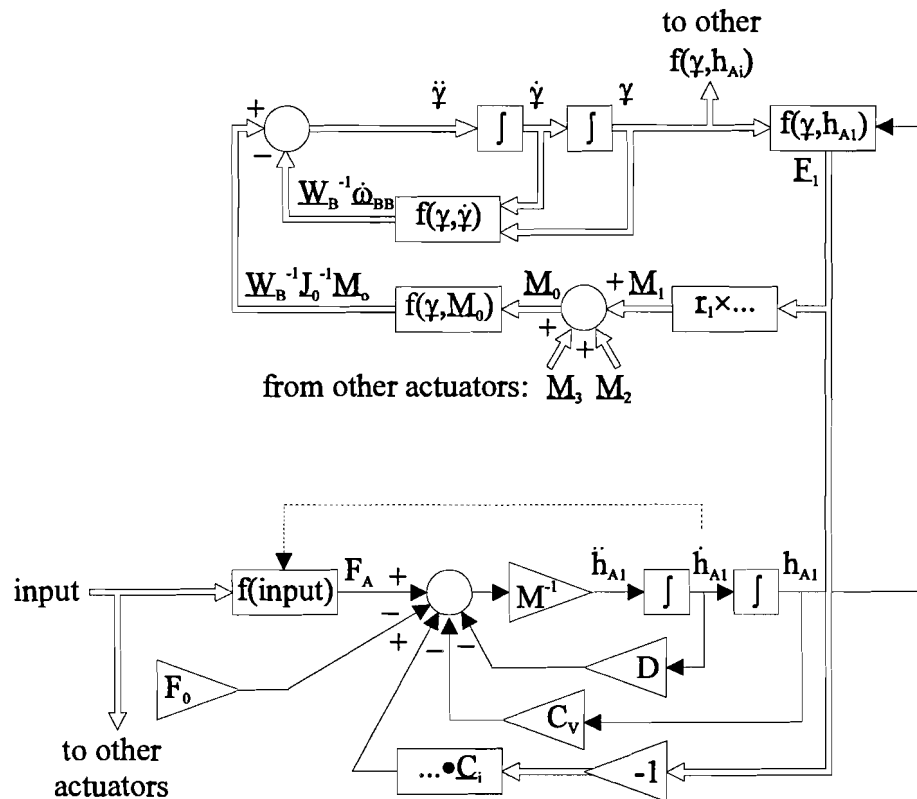


Figure 5.1: Block diagram of the simulation.

In the top part of Figure 5.1 the mirror dynamics are shown. In the bottom part one actuator is shown. For clarity the other actuators are omitted. The other actuators work in the same way as the one shown. Double line arrows indicate vectors, single line arrows indicate scalars.

The functions will now be described.

- $f(\gamma, h_{A1})$  Function that calculates the force  $E_1$  of the string on mirror arm 1, using  $\gamma$  and  $h_{A1}$  as inputs. In this block the following is done:
- $\Delta_1$  is calculated in local coordinates using  $R_B^T$ .
  - String vector  $a_i - \Delta_i$  is calculated in local coordinates.
  - Change in length  $a_i - \Delta_i - H$  is calculated.
  - String force due to change in length is calculated.
  - String force value  $F_i$  is calculated.
  - String direction is calculated.
  - String force  $E_i$  is calculated multiplying string direction and  $F_i$ .  $E_i$  is in local coordinates now.

- $f(\underline{\gamma}, \dot{\underline{\gamma}})$  Function calculating  $\underline{W}_B^{-1} \dot{\underline{\omega}}_{BB}$ , as described in (3.10).
- $f(\underline{\gamma}, \underline{M}_0)$  Function calculating  $\underline{W}_B^{-1} \underline{J}_0^{-1} \underline{M}_0$  as described in (3.10).
- $f(\text{input})$  Function calculating  $F_A$  using the input vector. If current control is used, the input vector  $\underline{I}$  contains the three currents through the actuators. If voltage control is used, the input vector  $\underline{U}$  contains the three actuator voltages. If voltage control is used, the extra input  $\dot{h}_{Ai}$  is needed, indicated by the dashed line. In the simulation voltage or current control can be chosen by setting a parameter. With this parameter also mixed control can be chosen. See appendix E, the MIRINI.M file.

The block diagram for the block  $f(\text{input})$  for current and voltage control is shown in Figure 5.2.

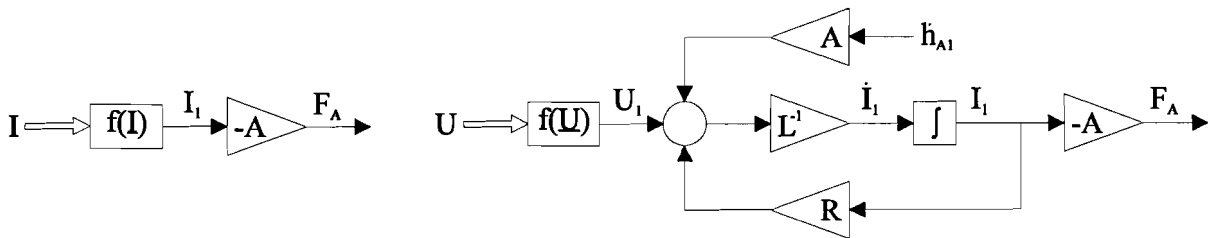


Figure 5.2: Block diagram of the input function.

On the left is the block diagram if current control is used, on the right is the block diagram if voltage control is used.

To the outside the mirror simulation has three inputs and three outputs:

- inputs: the three actuator inputs.
- outputs: the three Bryant angles.

## 5.1 Simulation characteristics

Only simulations were done using voltage control. This was partly due to time restrictions, but also because this system seems to be the best to use. By changing the pretensioning force, the "fastness" of the voltage controlled system can be controlled as shown in the previous chapter. Because of the damping of this system, the system is easier to control using voltage control. For these reasons voltage control is chosen. The voltage controlled system might be too slow for the tracking purposes it is designed for. In that case the current controlled system must be analyzed.

The simulations described further are simulations using voltage control.

Simulations were done to find some of the non-linear characteristics and to compare the non-linear simulation with the linearized model. To determine some characteristics several step response simulation were done. Two different type of step responses were done:

1. Step responses on each actuator: a step is put on one of the three actuators, and the response of the system is analyzed. The step response of every actuator is simulated.

2. Step responses of  $U_\psi$  and  $U_\theta$ : A step was put on each of these variables. The step on the actuators can then be described with (3.49). The response of the Bryant angles and sensor angles is analyzed.

Also tests were done to compare the linear model with the simulation.

### 5.1.1 Step responses of each actuator

In these simulations a step was put on one actuator. A step of 0.15 volt was used. The responses of the system are shown in Figure 5.3.

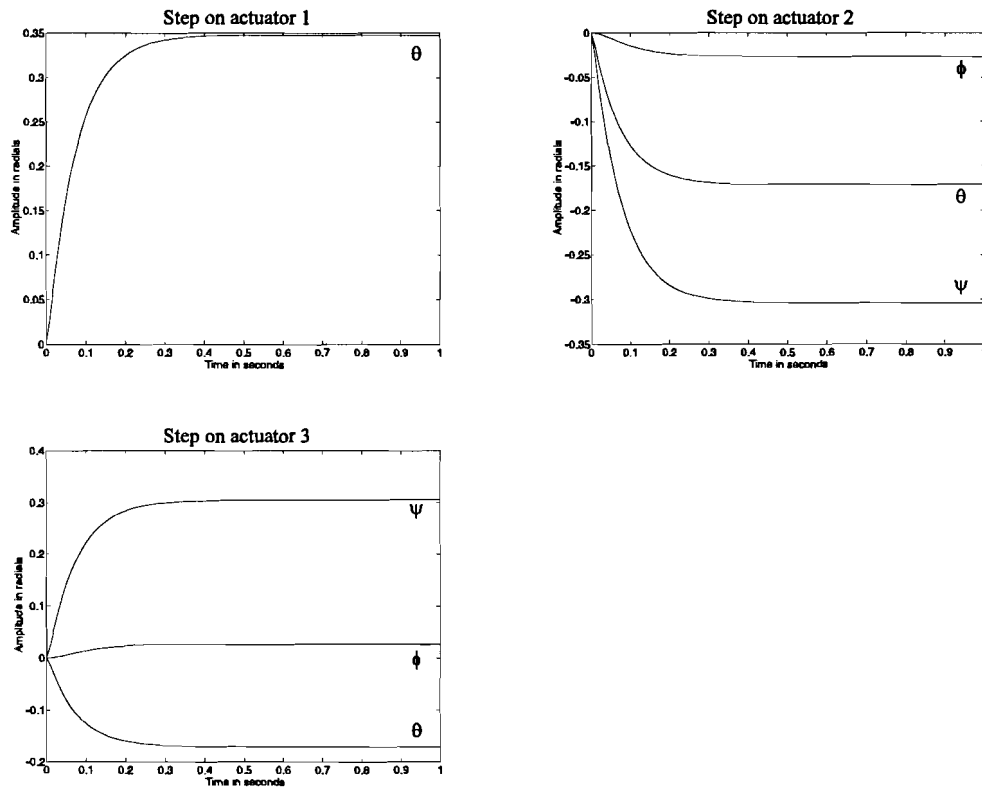


Figure 5.3: Step responses of the step on one actuator.

In the first plot of Figure 5.3, the step response of a step on actuator 1 is simulated. Only Bryant angle  $\theta$  is affected. The result is that mirror arm 1 moves downwards in the  $y=0$  plane. In the second plot, a step is put on actuator 2. All Bryant angles are affected. If the coordinates of the end of arm 2 are transformed to global coordinates using the Bryant angles, it can be verified that the movement of arm 2 is the same as the movement of arm 1 when a step was put on actuator 1: arm 2 moves downwards in the  $y = -\sqrt{3}\cdot x$  plane. The global  $y$  coordinates were verified to be the same. No rotations round the local or global  $z$  axes were present in the simulation.

The third plot concerns arm 3 and actuator 3. Here arm 3 move downwards in the  $y = \sqrt{3}\cdot x$  plane. Again no rotations round the local or global  $z$  axes were present in the simulation.

When a step is put on one actuator the rotation  $\phi$  remains small.

In all three plots, no overshoot is present.

### 5.1.2 Step responses using $U_\psi$ and $U_\theta$

In these simulations a step was put on the inputs  $U_\psi$  and  $U_\theta$ . The actual actuator inputs of the system can be calculated using (4.51). A step of 0.15 was put on  $U_\psi$  and  $U_\theta$ . First the response of a step on  $U_\psi$  will be discussed.

The response of a step of 0.15 on  $U_\psi$  is shown in Figure 5.4.

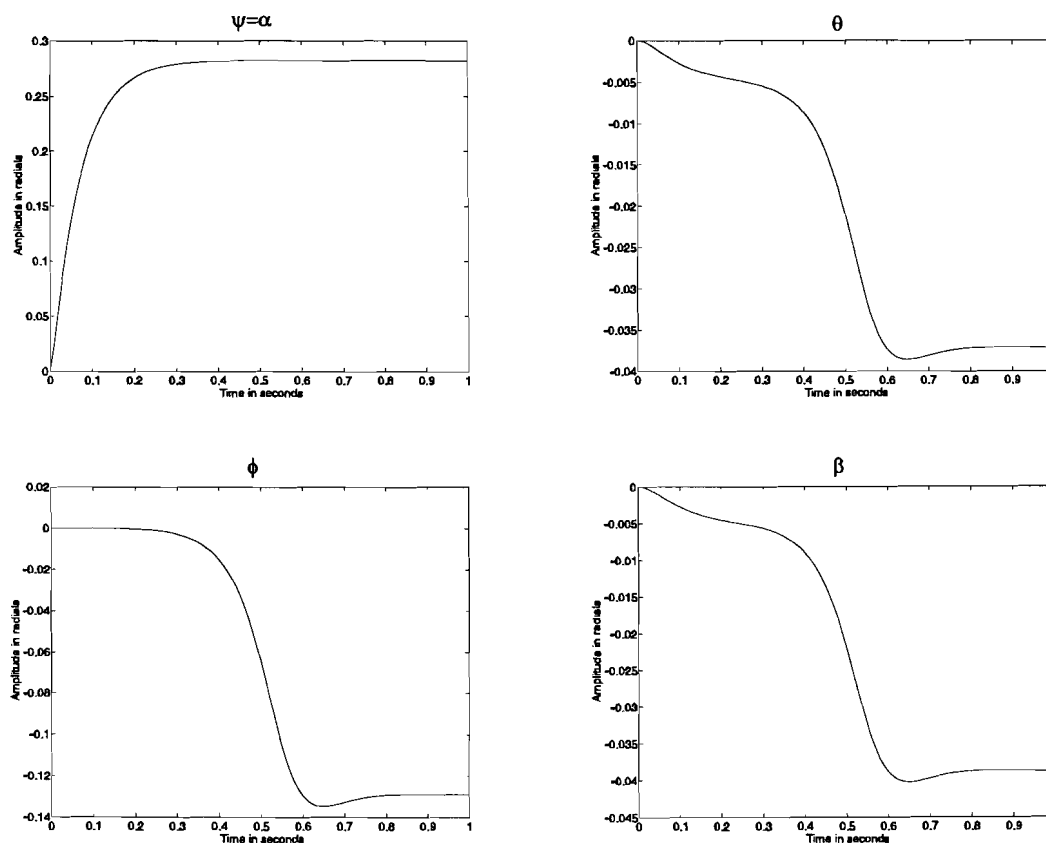


Figure 5.4: Step response on  $U_\psi$ .

In Figure 5.4 the response of the Bryant angles  $\psi$ ,  $\theta$  and  $\phi$  are shown as well as the sensor angle  $\beta$ , sensor angle  $\alpha$  is the same as Bryant angle  $\psi$ . All angles are effected by the step. The response of  $\psi$  is the most significant, as was expected. Bryant angles  $\theta$  and  $\phi$  are also affected. This can be explained when looking at the mirror layout. When the mirror is rotated round the x-axis, then this does not only cause a momentum round the x-axis, but also round the y-and z-axis. This affects all the angles involved.

In this case the rotation  $\phi$  is significant. This means that the linear model does accurately describe the situation.

The settling time of  $\psi$  is about 0.5 seconds. This however is not the settling time of the normal of the mirror. This can be seen by looking at the sensor angle  $\beta$ . This angle settles



after about 0.8 seconds. The open loop bandwidth of the system using this settling comes to 1.25 Hz.

The step response of a step on  $U_\theta$  will now be discussed. The step response is shown in Figure 5.5.

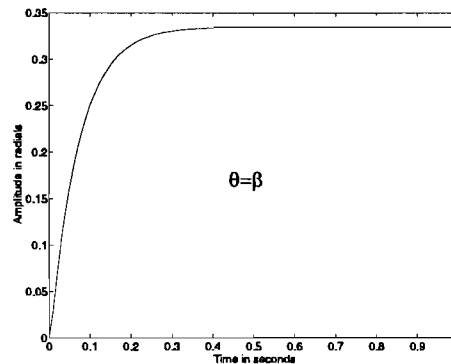


Figure 5.5: Step response on  $U_\theta$ .

When a step is put on  $U_\theta$ , only the Bryant angle  $\theta$  is affected, the other Bryant angles remain zero. If the other Bryant angles are zero, it means that only sensor angle  $\beta$  is affected. The reason that only  $\theta$  is affected is that if the mirror is rotated around the y-axis, only a momentum round the y-axis is caused. The resulting momentum round the x- and z-axis remain zero. The result is a response similar to that if only actuator 1 is used.

From the equilibrium position  $U_\theta$  does not affect the other angles.  $U_\psi$  affects  $\psi$ , but also the other angles.

### 5.1.3 Comparing the linear system with the simulation

In this section it will be tested whether the simulation corresponds with the linear model for small angles. For the inputs of the linear system the inputs  $U_\psi$  and  $U_\theta$  will be used. The same inputs will be applied to the simulation. In order to keep the angles small, a small input will be applied. For  $U_\psi$  and  $U_\theta$  a sine signal is chosen with amplitude 0.01 and the frequency will be that of the cutoff frequency: 2.4 Hz.

The linearity of the simulation will also be tested for larger angles. The same inputs will be used, only the amplitude in this experiment will be 0.15 for both inputs.

It is expected that if input  $U_\theta$  is applied, the simulation will have a relative larger response for larger angles than if input  $U_\psi$  is applied. This is because input  $U_\theta$  only effects output  $\theta$ , and all the energy of the input goes into the excitation of  $\theta$ . Input  $U_\psi$  not only effects  $\psi$ , put also the other Bryant angles. The effect on the other angles will cause the input energy to be divided over all angles, so the amplitude of  $\psi$  will be relatively less than that of  $\psi$ . For small angles the system should follow the linear model.

In Figure 5.6 the simulation response of  $U_\psi$  on  $\psi$  and of  $U_\theta$  on  $\theta$  are shown, together with the linear response to the same input. The input amplitude is 0.01, keeping the angles small. The linear response has been made thicker and grey to allow the signals to be distinguished.

It can be seen that the simulation follows the linear response for small angles.

In Figure 5.7 the simulation response of  $U_\psi$  on  $\psi$  and of  $U_\theta$  on  $\theta$  is shown, together with the linear response using the same input. The input amplitude is 0.15, so the response is larger. Again the linear response has been made thicker and grey to distinguish the signals. It can be seen that for larger angles the simulation response is larger than the linear response. It can also be seen that the response of  $\psi$  is less than the response  $\theta$ , as was expected.

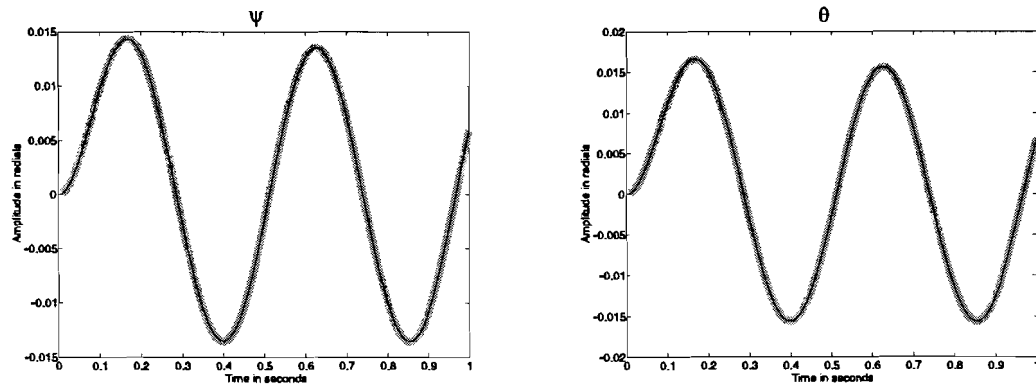


Figure 5.6: Simulation and linear response on  $U_\psi$  and  $U_\theta$  for small angles.

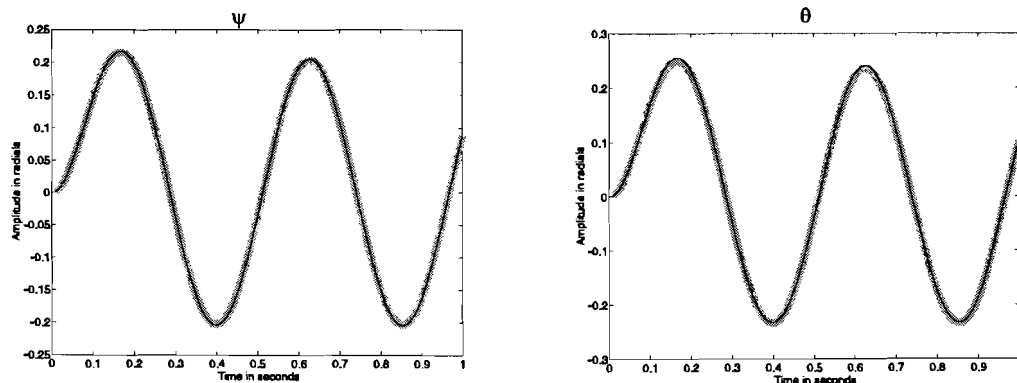


Figure 5.7: Simulation and linear response on  $U_\psi$  and  $U_\theta$  for large angles.

## 6. Identification of the simulation

A simulation model is identified using the Minimal Polynomial Identification toolbox MPI, developed by Heinz Falkus [4]. The simulation described in the previous chapters is used to generate the input output data. Sensor noise is added to the output data. The sensor is accurate to 0.1%. For this reason noise is added to the signal, so that the signal noise ratio of the output data is 80 dB. The added noise is zero mean normally distributed white noise.

The outputs are the sensor angles  $\alpha$  and  $\beta$ , since these are the angles that define the normal to the mirror. The normal is the parameter that determines the path of the laser beam. The inputs used in the identification are  $U_\psi$  and  $U_\theta$ , because in the linear case they independently control the sensor angles by two SISO transfer functions. Using  $U_\psi$  and  $U_\theta$  the system will be strongly decoupled. The identification will therefore be a MIMO identification, with 2 inputs and 2 outputs.

From the step responses of  $U_\psi$  and  $U_\theta$  it was shown that if only  $U_\theta$  is excited, this only has an effect on  $\theta$ . A step on  $U_\psi$  excites  $\psi$  the most, but the other angles are also influenced. The decoupling is still strong though.

The input to  $U_\psi$  and  $U_\theta$  will be two uniformly distributed noise series. These input datasets generated using Matlab. The input datasets are sampled by a zero-order hold before they are led into the system. The sample frequency of the zero-order hold is chosen the same as the sample frequency of the output.

A schematic view of the system, system inputs and outputs, and identification inputs and outputs is shown in Figure 6.1.

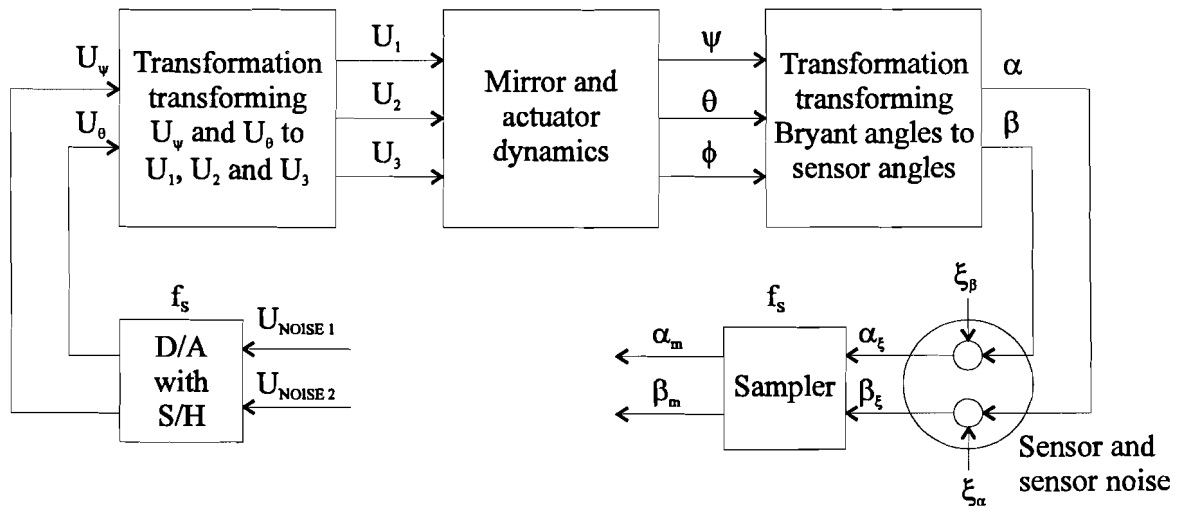


Figure 6.1: Schematic view of the identification.

The process plus disturbance in Figure 6.1 is from the inputs  $U_1$ ,  $U_2$  and  $U_3$  to the outputs  $\alpha_\xi$  and  $\beta_\xi$ . This is what normally the real system would be.

The identification will be performed on the system as shown.

## 6.1 Model structure and the minimization criterion

The general model structure is given by [1],[2]:

$$A(z^{-1})Y_{k,i} = \frac{B_{i1}(z^{-1})}{F(z^{-1})}U_{k-nk_{i1},1} + \dots + \frac{B_{inu}(z^{-1})}{F(z^{-1})}U_{k-nk_{iu},nu} + \frac{C_{ii}(z^{-1})}{D(z^{-1})}\Xi_{k,i} \quad (6.1)$$

where

$$Y \in \mathcal{R}^{N \times ny}, U \in \mathcal{R}^{N \times nu}, \Xi \in \mathcal{R}^{N \times ny} \quad (6.2)$$

describe the input/output data and the independent white noise sequences for  $N$  data samples of a multi variable system with  $nu$  inputs and  $ny$  outputs.

From Figure 6.1 it can be seen that the noise is additive noise to the outputs. Therefore an output error (OE) model is chosen for the identification. The model used for the identification becomes:

$$Y_{k,i} = \frac{B_{i1}(z^{-1})}{F(z^{-1})}U_{k-nk_{i1},1} + \dots + \frac{B_{inu}(z^{-1})}{F(z^{-1})}U_{k-nk_{iu},nu} + \Xi_{k,i} \quad (6.3)$$

The polynomials are defined as:

$$B_{ij} = b_{ij,1} + b_{ij,2}z^{-1} + \dots + b_{ij,nb_{ij}}z^{-nb_{ij}+1} \quad i = 1 \dots ny, j = 1 \dots nu \quad (6.4)$$

$$F(z^{-1}) = 1 + f_1z^{-1} + \dots + f_{nf}z^{-nf}$$

All polynomials coefficients can be combined in a parameter vector  $\Theta$  defined by:

$$\Theta = [b_{11,1} \dots b_{11,nb_{11}} \ b_{12,1} \dots b_{ny,nu,nb_{ny,nu}} \ f_1 \ f_{nf}]^T \quad (6.5)$$

The predictor is defined as:

$$\hat{Y}_{k,i}(\Theta) = \frac{1}{F(z^{-1})} [B_{i1}U_{k-nk_{i1},1} + \dots + B_{inu}U_{k-nk_{iu},nu}] = W_{k,i}(\Theta) \quad (6.6)$$

The prediction error for an OE model the prediction error becomes:

$$E_{k,i}(\Theta) = Y_{k,i} - \hat{Y}_{k,i} = Y_{k,i} - W_{k,i}(\Theta) \quad (6.7)$$

Define the maximum delay required for initialization by:

$$n = \max_{i,j}([nb_{ij} + nk_{ij} - 1 \ nf]) \quad (6.8)$$

and introduce the following regression matrices:

$$\Phi_{U_i} = \begin{bmatrix} U_{n-nk_{ij}+1,j} & \dots & U_{n-nk_{ij}-nb_{ij}+1,j} \\ \vdots & & \vdots \\ U_{N-nk_{ij}+1,j} & \dots & U_{N-nk_{ij}-nb_{ij}+1,j} \end{bmatrix}, \Phi_{W_i}(\Theta) = \begin{bmatrix} -W_{n,i} & \dots & -W_{n-nf+1,i} \\ \vdots & & \vdots \\ -W_{N,i} & \dots & -W_{N-nf+1,i} \end{bmatrix} \quad (6.9)$$

The predictor can now be written in a pseudolinear regression form [3] [4]:

$$\hat{Y}_v(\Theta) = \Phi(\Theta)\Theta \quad (6.10)$$

where

$$\hat{Y}_v(\Theta) = [\hat{Y}_{1,1}(\Theta) \dots \hat{Y}_{N-1,1}(\Theta) \ \hat{Y}_{1,2}(\Theta) \dots \hat{Y}_{N-n,ny}(\Theta)]^T \quad (6.11)$$

and

$$\Phi(\Theta) = \begin{bmatrix} \phi_{U_{11}} & \cdots & \phi_{U_{1nu}} & 0 & \cdots & 0 & 0 & \cdots & \cdots & 0 & 0 & \phi_{W_1}(\Theta) \\ 0 & \cdots & 0 & \phi_{U_{21}} & \cdots & \phi_{U_{2nu}} & \ddots & & & & \vdots & \phi_{W_2}(\Theta) \\ \vdots & & \vdots & 0 & \cdots & 0 & \ddots & & & & \vdots & \vdots \\ \vdots & & \vdots & \vdots & & \vdots & \ddots & 0 & \cdots & \cdots & 0 & \vdots \\ 0 & \cdots & 0 & 0 & \cdots & 0 & 0 & 0 & \phi_{U_{ny1}} & \cdots & \phi_{U_{nynu}} & \phi_{W_{ny}}(\Theta) \end{bmatrix} \quad (6.12)$$

The prediction error for multivariable systems when using a minimal polynomial model structure in vector form is given by:

$$E_v = Y_v - \hat{Y}_v \quad (6.13)$$

For prediction error minimization the normalized loss-function is:

$$J_E(\Theta) = \frac{1}{N_v} E_v^T E_v \quad (6.14)$$

where  $N_v = ny(N-n)$  in a least squares criterion. The criterion is valid only if the white noise sequences disturbing the process are mutually independent and that the input-output data is scaled in such a way that the white noise sequences have equal variance. The minimization method used to minimize (6.14) can be found in [4], resulting in the estimator  $\Theta$ .

## 6.2 Experiment design

The input to  $U_\psi$  and  $U_\theta$  are noise series. These series are uniformly distributed white noise series. The series are created in Matlab.

### 6.2.1 Data collection sample frequency

The sample frequency with which the data is collected, is set by the time step in the simulation. For voltage control the time step is chosen to be  $1 \cdot 10^{-5}$  seconds. This time step gives a reliable simulation run. This means that the data collection sample frequency is 100 kHz.

### 6.2.2 Identification sample frequency $f_s$

A practical choice for the sample frequency [3] is:

$$10f_B \leq f_s \leq 30f_B \quad (6.15)$$

$f_B$  is the bandwidth of the process, and is defined as the cutoff frequency. From the linear Bode plots it is found that the cutoff frequency is at about 2.4 Hz. If this criterion is used, the identification frequency should be between 24 Hz and 72 Hz. Knowledge of the poles of the linear system can also be used to determine  $f_s$ . The second slowest pole is at  $\omega = -2.8966 \cdot 10^2$  rad/s or  $f = 46.1$  Hz. To correctly identify this pole also, the sampling rate should be at least twice this frequency. For this reason  $f_s$  is chosen 100 Hz. By reducing the data collection frequency by a factor 1000,  $f_s$  is reached.

In order to perform delay-time corrections, it is necessary to analyse the cross-correlations between inputs and outputs. The cross-correlations are calculated on data sampled at 10 times

the identification frequency [1]. This frequency is reached by reducing the collection frequency by a factor 100.

### **6.2.3 Determining experiment duration**

The experiment duration should be 5 to 10 times the largest relevant time constant. The largest relevant time constant is about 3 times the settling time of the process [1]. The settling time can be determined from the simulation of the step responses. The settling time is about 0.8 seconds. The experiment duration should be between about 4 and 8 seconds. The experiment duration is set at 5 seconds.

## **6.3 Data preprocessing**

Data preprocessing is concerned with handling the data before estimating. It concerns input and output data of the process. In case of the simulation the output is not simulated process output: noise has to be added first. The simulation output is added with noise, setting the signal noise ratio of the output at 80 dB. Simulation output added with this noise is the simulated process output. The preprocessing steps of process input and output will be described in this section.

### **6.3.1 Sample rate reduction**

In case of the simulation the input and output data sample rate has to be reduced to 10 times  $f_s$ , before further processing. Before the actual identification the sample rate should again be reduced to  $f_s$ . An anti aliasing filter should be applied while doing so. Matlab provides tools for sample rate reduction.

### **6.3.2 Detrending and peak shaving**

The output of a process experiment should undergo detrending and peak shaving. Peaks occur in the output through for example switching behaviour of high power process machinery. In the case of the simulation, no spikes are present, so peakshaving is not necessary.

No trend is present in the simulation. The mean of the input signal should be zero, since this is zero mean white noise. Because of the absence of trend, the output signal should be zero mean also. Because the mean might not be exactly zero, the mean of the signals should be removed.

### **6.3.3 Delay time correction**

In real processes considerable time delays may occur in the output signals. If the signals are not corrected for the delays, they have to be estimated as part of the model. Delay times can be determined by cross-correlation analysis of all inputs and outputs. The MPI toolbox provides tools for the cross-correlation analysis. Cross correlation analysis is done at 10 times  $f_s$ . In this identification of a simulation, no such delay times are present. The only delay time present, is the delay time of the simulation: this delay time is 1 time step, which is  $1 \cdot 10^{-5}$  seconds.

### **6.3.4 Signal scaling**

The input/output data should be scaled in such a way that the white noise sequences disturbing the process have equal variance to avoid relative weighting. An accurate estimate can be obtained by estimating a high order ARX-model. A high order ARX model can approximate any linear system well for sufficiently high order. The standard deviation of the prediction error computed from the ARX model can be used as scaling factors. The scaling has to be verified after completing model estimation.

## **6.4 Model estimation**

Model structure has already been selected: the selected structure is an OE model. The order of the model has to be determined also. This can be done by loss function analysis. If the loss function is plotted to the model order, the order can be estimated.

## **6.5 Model validation**

In the validation phase, the estimated model is checked. In this section the ways used to validate the model are discussed.

### **6.5.1 Correlation between inputs and residuals**

If the model is estimated correctly, the cross correlation between inputs and residuals should be white. If the residuals are white all information in the residuals is explained by the estimated model.

### **6.5.2 Comparing real and estimated output**

The real output in this case is the process output of the simulation. The estimated outputs are the simulated output using the estimated model. If the outputs resemble, this is an indication that the model is correct.

The identification process described above will be applied to the system. The results are described in the next chapter.

## 7. Identification results

The identification is carried out as described in the previous chapter. One second of the input and output data is shown in Figure 7.1. The sampled inputs, and the outputs are shown. One

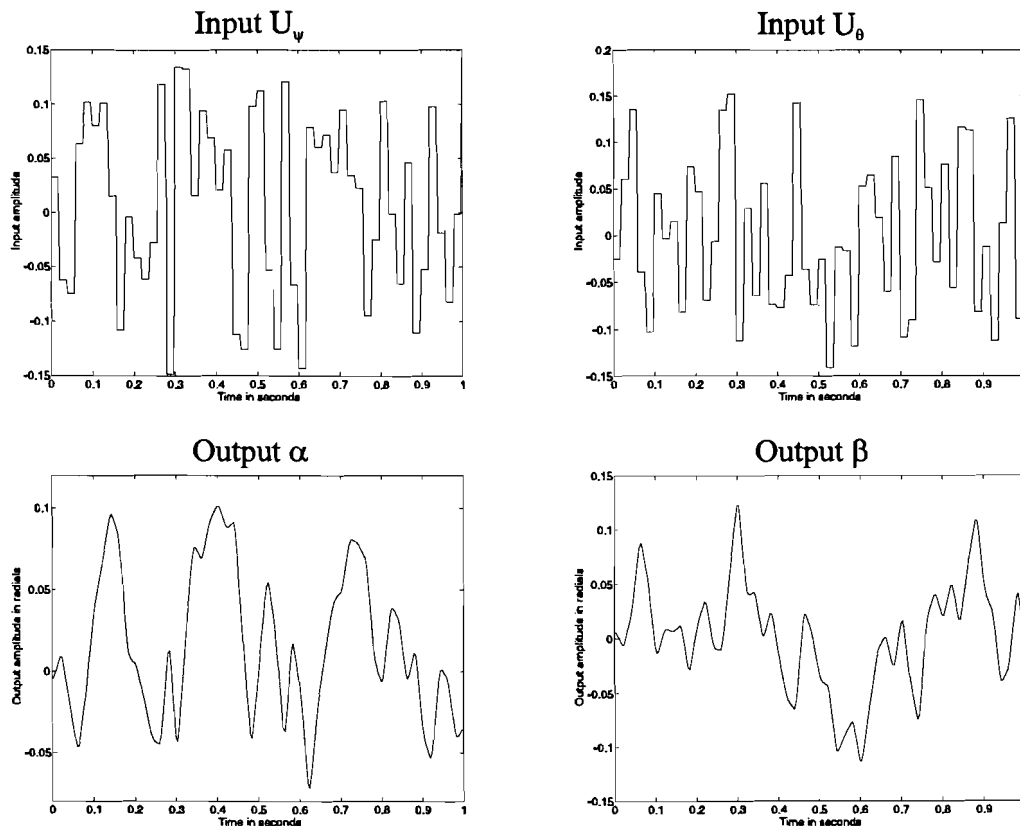


Figure 7.1: Input and output data.

data set of 10 seconds is generated. This set is split in a identification and validation part, as will be described later in this chapter. The steps of the actual identification will be described in this chapter.

### 7.1 Data preprocessing

Noise is added to the data from the simulation shown in Figure 7.1. The noise is added so that the signal noise ratio of the outputs are 80 dB. This is done by scaling the noise so that the standard deviation ratio of the output signal and the noise is 80 dB.

Next the simulation sample frequency determined by the step size of the simulations reduced to 10 times the identification sampling frequency  $f_s$ . In this step, the first simulation sample is discarded, to correct the signal from the one step time delay caused by the simulation. This is only a delay of 10 ms. The step time of the simulation is set at  $1 \cdot 10^{-5}$  seconds, corresponding to a frequency of 100 kHz. The reduction is done using the Matlab function DECIMATE, using a FIR filter.

The next steps of the identification can be performed with the MPI identification tool [4].



### 7.1.1 Peakshaving and detrending

Detrending and peak shaving is not necessary for the simulation results. The MPI identification tool provides the functions to do this, but this resulting signals which are the same as the unprocessed signals. The input and output signals were mean corrected. Theoretically the signals should have zero mean, but the signals proved to have a little offset. The offset is subtracted from the signals. The MPI tool which performs peakshaving and detrending is MPI\_DET.

### 7.1.2 Delay time correction

No delays should be present in the output signals. In order to verify this, the cross-correlations between all inputs and outputs over the estimation data set is computed. The resulting cross-correlations are depicted in Figure 7.2. The vertical bars indicate the oversampling ratio, so the delay times can be determined at a multiple of the identification frequency. The oversampling ratio used in is 10.

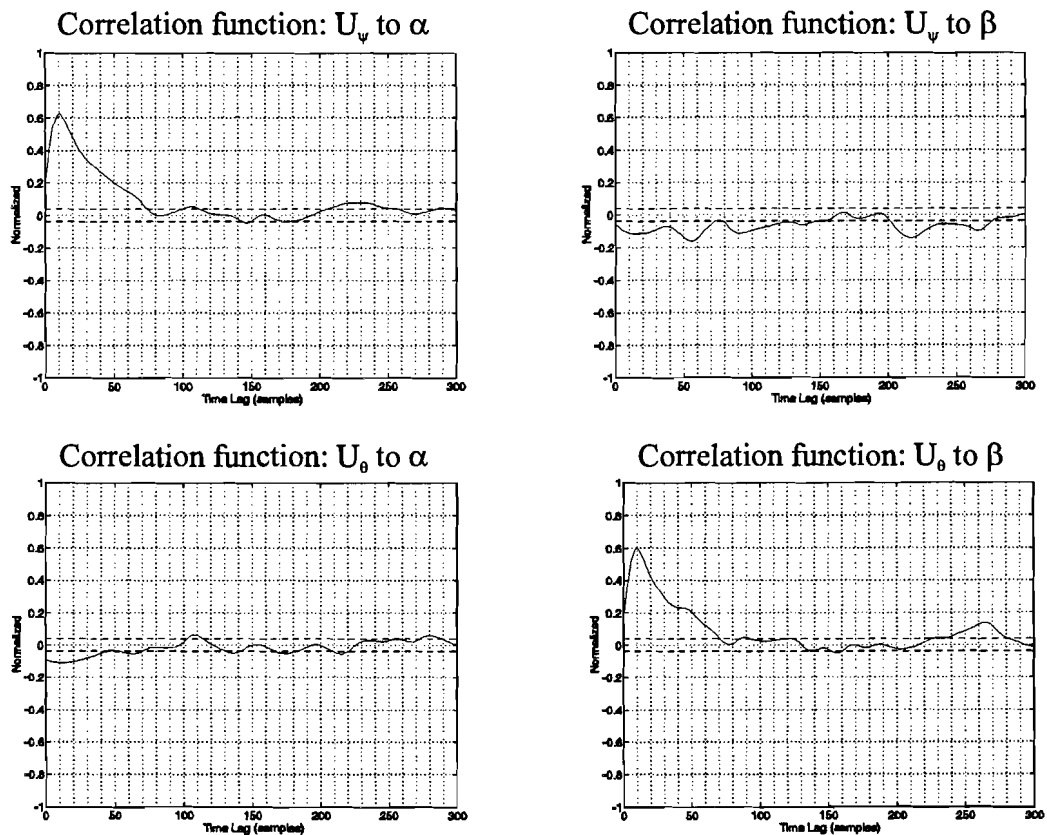


Figure 7.2: Cross correlations between inputs and outputs.

The 95% confidence interval is also shown. It can clearly be seen that there are no delays between input  $U_\psi$  and outputs  $\alpha$ , and between input  $U_\theta$  and output  $\beta$ . The correlations between  $U_\psi$  and  $\beta$ , and between  $U_\theta$  and  $\alpha$  not very correlated. Still some correlation is visible, and it can be concluded that no delays are present. The fact that the system is uncorrelated

between  $U_\psi$  and  $\beta$ , and between  $U_\theta$  and  $\alpha$  is an indication that the system can be described by two SISO functions. No delay time correction is done.

The MPI tool used for calculating the cross-variance is MPI\_CC, and the tool performing delay time correction is MPI\_DC.

### 7.1.3 Sample rate reduction to $f_s$ and normalization

The next step of the data preprocessing is the sample rate reduction. Also the data set is split in an estimation set and a validation set of both 5 seconds. The sampling frequency is reduced by 10 to  $f_s$ , the identification sample frequency of 100 Hz. The estimation and validation data set length is therefore 500 samples.

In the same step the estimation data is normalized so that the standard deviation of the input and output data equals 1. This is done by scaling. Scaling has to be applied a second time in such a way that the white noise sequences disturbing the system have equal variance. This step is described in the next paragraph.

The MPI tool for sample rate reduction to the identification frequency and normalization is MPI\_DRN.

The scaling factors for the inputs and outputs are given in Table 7-1.

Table 7-1: Normalization scaling factors.

	Input		Output	
	$U_\psi$	$U_\theta$	$\alpha$	$\beta$
Scaling factor	19.189	16.857	11.929	12.034

### 7.1.4 Equal variance scaling

For minimal polynomial model identification it is necessary that the input/output data is scaled in such a way that the white noise variance disturbing the system have equal variance. If this is not done a relative weighting will be done during the identification. Normally, the white noise variances are not known.

A linear system can be described well by an ARX model of sufficiently high order. The scaling factors can be calculated using the standard deviation of the prediction error computed from the high order ARX model. The scaling factors for each output are proportional to the inverse of the standard deviation of the prediction error of the output.

A high order ARX model of the scaled data can be used to check if the standard deviations of the prediction error is equal. The scaling has to be verified after completing the actual identification model.

In this identification a 50<sup>th</sup> order ARX model is used.

The high order ARX model estimation is done using the MPI tool MPI. The prediction error of the high order model is calculated using MPI\_PE.

The variances of the prediction error before and after scaling are given in Table 7-2. The scaling factors of the outputs are also given.

Table 7-2: Equal variance scaling parameters.

	Prediction error variance before scaling	Prediction error variance after scaling	Scaling factor
Output $\alpha$	0.0051	0.0045	0.8675
Output $\beta$	0.0044	0.0043	1

It can be seen that the prediction error variances of the scaled high order model are about equal.

The parameters of the identified model are based on the scaled inputs and outputs. The parameters have to be corrected for the scaling afterwards.

## 7.2 Model estimation

An OE model is estimated for the system. The order is determined by looking at the loss function. Models have been calculated from 0<sup>th</sup> order to 8<sup>th</sup> order. The loss function of the models versus the model order is shown in Figure 7.3.

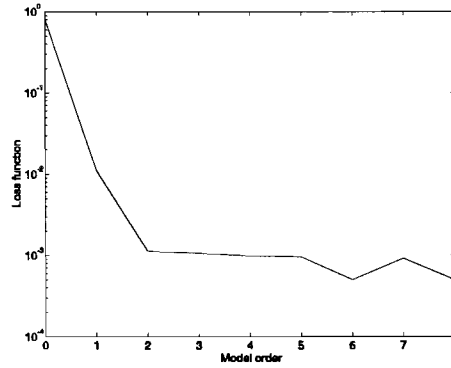


Figure 7.3: The loss function versus model order.

It is clear that the model order should be 2.

Theoretically the loss function should be decreasing for increasing model order. This is not always the case due to the fact that the global minimum of the criterion function can not always be found, and that the minimization terminates in a local minimum. This is the case for the model with order 7.

The MPI tool used to identify the models is MPI.

The results for the identified second order system are:

$$\alpha(k) = \frac{-1.0715 \cdot 10^{-4} + 1.6889 \cdot 10^{-1} z^{-1} + 7.1175 \cdot 10^{-2} z^{-2}}{1 - 9.2555 \cdot 10^{-1} z^{-1} + 5.4308 \cdot 10^{-2} z^{-2}} U_{\psi}(k) + \frac{-5.3592 \cdot 10^{-4} - 2.8551 \cdot 10^{-3} z^{-1} + 3.3107 \cdot 10^{-3} z^{-2}}{1 - 9.2555 \cdot 10^{-1} z^{-1} + 5.4308 \cdot 10^{-2} z^{-2}} U_{\theta}(k) \quad (7.1)$$

$$\beta(k) = \frac{9.737 \cdot 10^{-4} + 2.7632 \cdot 10^{-3} z^{-1} + 3.2568 \cdot 10^{-3} z^{-2}}{1 - 9.2555 \cdot 10^{-1} z^{-1} + 5.4308 \cdot 10^{-2} z^{-2}} U_{\psi}(k) + \frac{1.030 \cdot 10^{-3} + 1.9247 \cdot 10^{-1} z^{-1} + 8.3855 \cdot 10^{-2} z^{-2}}{1 - 9.2555 \cdot 10^{-1} z^{-1} + 5.4308 \cdot 10^{-2} z^{-2}} U_{\theta}(k) \quad (7.2)$$

The Z-transformations of (7.1) and (7.2) are transformed to Laplace transforms. This is done using Matlab. The equations are processed using a zero-hold correction, for a sample frequency of 100 Hz. The resulting Laplace transforms are:

$$\alpha(s) = \frac{-1.0715 \cdot 10^{-4} s^2 - 1.0598s + 7.6177 \cdot 10^3}{s^2 + 2.9113 \cdot 10^2 s + 4.0875 \cdot 10^3} U_\psi(s) + \frac{-5.3592 \cdot 10^{-4} s^2 + 3.0248 \cdot 10^{-1} s - 2.1275 \cdot 10^2}{s^2 + 2.9113 \cdot 10^2 s + 4.0875 \cdot 10^3} U_\theta(s) \quad (7.3)$$

$$\beta(s) = \frac{9.7372 \cdot 10^{-4} s^2 - 1.2767 \cdot 10^{-1} s + 2.2202 \cdot 10^2}{s^2 + 2.9113 \cdot 10^2 s + 4.0875 \cdot 10^3} U_\psi(s) + \frac{1.030 \cdot 10^{-3} s^2 - 1.4023 \cdot 10^{-1} s + 8.8046 \cdot 10^3}{s^2 + 2.9113 \cdot 10^2 s + 4.0875 \cdot 10^3} U_\theta(s) \quad (7.4)$$

Let  $B_{ij}$  be the numerator polynomial of the transfer function of input  $i$  to output  $j$ . The roots of this polynomial gives the zeros of the corresponding transfer function. The roots of the denominator polynomial  $F$  give the poles of the system. The roots of the polynomials are given in Table 7-3 for both the time discrete and the time continuous case.

Table 7-3: Roots of the  $F$  and  $B$  polynomials.

	Time discrete		Time continuous	
	$F$	$8.6259 \cdot 10^{-1}$	$6.2959 \cdot 10^{-2}$	$-2.7653 \cdot 10^2$
$B_{11}$	$1.5767 \cdot 10^3$	$-4.2131 \cdot 10^{-1}$	$-1.4720 \cdot 10^4$	$4.8297 \cdot 10^3$
$B_{12}$	$-3.6218$	$-1.7056$	$2.8220 \cdot 10^2 + 5.6333 \cdot 10^2 j$	$2.8220 \cdot 10^2 - 5.6333 \cdot 10^2 j$
$B_{21}$	$-1.4189 + 1.1539j$	$-1.4189 - 1.1539j$	$6.5556 \cdot 10^1 + 4.7298 \cdot 10^2 j$	$6.5556 \cdot 10^1 - 4.7298 \cdot 10^2 j$
$B_{22}$	$-1.8635 \cdot 10^2$	$4.3671 \cdot 10^{-1}$	$6.8042 \cdot 10^2 + 2.8428 \cdot 10^3 j$	$6.8042 \cdot 10^2 - 2.8428 \cdot 10^3 j$

It can be seen that the two slowest poles of the linear model are nearly the same as those of the estimated system.

The transfer function from  $U_\psi$  to  $\alpha$  and the transfer function from  $U_\theta$  to  $\beta$  should show considerable symmetry. The zeros of these functions are the roots of the  $B_{11}$  and  $B_{22}$  polynomials. When looking at the zeros the symmetry cannot be found. The symmetry is lost because of the difference in estimation of the first factor of the  $B_{11}$  and  $B_{22}$  polynomials. This factor is relatively small. In the  $B_{11}$  polynomial this factor is estimated negative, in the  $B_{22}$  polynomial this factor is estimated positive. If these factors were estimated the same, the symmetry would show up. If, in the time continuous case, the first factor of the  $B_{11}$  polynomial would have been estimated the same as that of the  $B_{22}$  polynomial, the roots of  $B_{11}$  would change considerably. The roots in this case can be seen in Table 7-4. The roots are the time-continuous roots.

Table 7-4: Roots of the  $B_{11}$  and  $B_{22}$  polynomials.

$B_{11}$	$5.1423 \cdot 10^2 + 2.6699 \cdot 10^3 j$	$5.1423 \cdot 10^2 - 2.6699 \cdot 10^3 j$
$B_{22}$ (unchanged)	$6.8042 \cdot 10^2 + 2.8428 \cdot 10^3 j$	$6.8042 \cdot 10^2 - 2.8428 \cdot 10^3 j$

The symmetry in this case is much more clear. In the same way this can be done the other way around. The roots of the polynomials, if the first factor of the  $B_{22}$  polynomial would have been

estimated the same as the first factor of the  $B_{11}$  polynomial, can be seen in Table 7-5. Now the roots of  $B_{11}$  remain the same.

Table 7-5: Roots of the  $B_{11}$  and  $B_{22}$  polynomials.

$B_{11}$ (unchanged)	$-1.7724 \cdot 10^4$	$4.6364 \cdot 10^3$
$B_{22}$	$-1.4720 \cdot 10^4$	$4.8297 \cdot 10^3$

Again the symmetry is clear. The first factor of the polynomials is relatively small. Because of the 'smallness', the factor is estimated with a different sign for  $B_{11}$  and  $B_{22}$ . The fact that it is estimated with a different sign doesn't mean that the identification results are unreliable. The zeros are far from the poles for  $B_{11}$  and  $B_{22}$ , so the influence of the zeros is only slight.

The impulse response can be analyzed to check the validity of the model.

The cross-correlation between the input and output of a system excited with inter-channel zero mean white noise can be given by [1]:

$$\Psi_{yu}(\tau) = \sigma^2(u) \cdot M_\tau \quad (7.5)$$

Here  $\sigma^2(u)$  is the variance of the input signal and  $M_\tau$  are the elements of the impulse response. By scaling the cross-correlation with the variance of the input signal the impulse response can be calculated. This impulse response can be compared with the impulse response of the identification using the estimated discrete transfer function.

The scaled cross-correlation of the inputs  $U_\psi$  and  $U_\theta$  to the outputs  $\alpha$  and  $\beta$  are shown in Figure 7.4. The impulse responses of the estimated discrete transfer functions of  $U_\psi$  to  $\alpha$ , and of  $U_\theta$  to  $\beta$  are also shown.

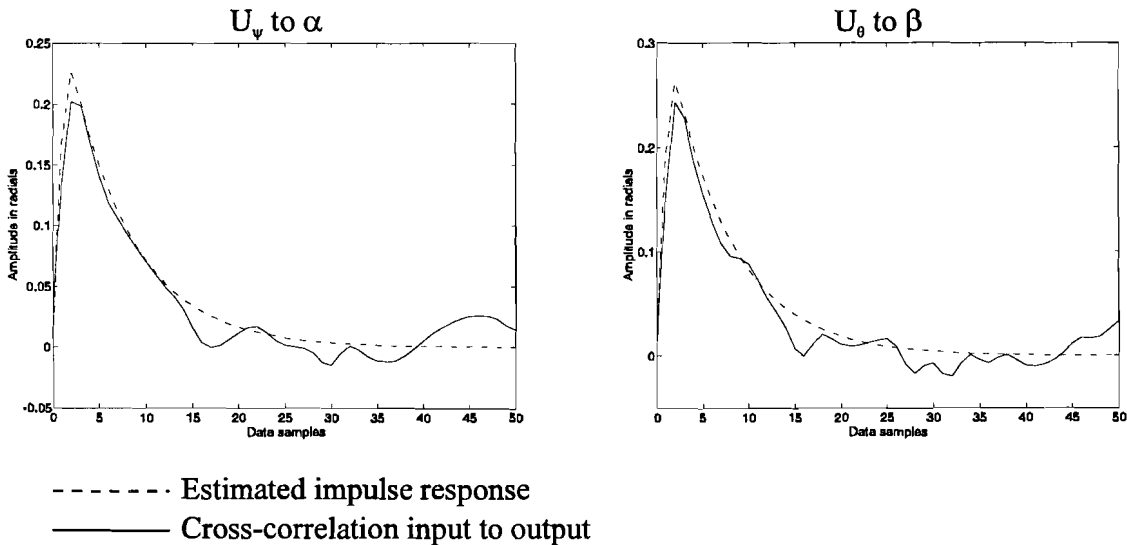


Figure 7.4: Scaled cross-correlations between inputs and outputs, and estimated impulse responses.

It can be seen that the impulse responses match reasonably well, indicating that the identification results are reliable. The inter-channel influence is very small as can be seen from factors of the  $B_{12}$  and  $B_{21}$  polynomials. These factors are small compared to the factors of  $B_{11}$  and  $B_{22}$ . In the next section it will be shown that the influence is negligible. The impulse responses of those transfers are omitted for this reason.

The linear model derived in chapter 4 follows the non-linear model reasonably well. If the impulse responses of the linear model and the estimated model are alike, then this is an indication that the identification is reliable. The impulse responses of the linear model and the estimated time-continuous model are shown in Figure 7.5.

Here the impulse responses are practically identical. Again this is an indication that the identification results are reliable. The impulse response of the linear system are displayed with a thick line to allow better distinction.

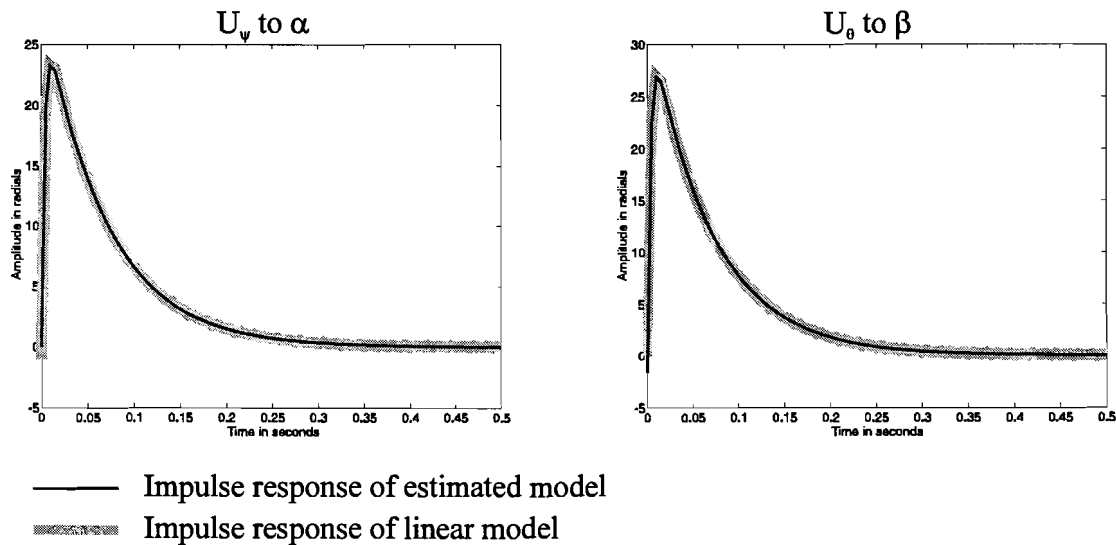


Figure 7.5: Impulse responses of the linear model and the estimated time continuous model.

### 7.3 Model validation

For correct identification the variance of the prediction error of both outputs should be equal.

The variance of the prediction error of output 1 and 2 are:

Prediction error variance output 1:  $1.279 \cdot 10^{-5}$

Prediction error variance output 2:  $1.138 \cdot 10^{-5}$

The variances are of approximately the same size indicating correct scaling.

The cross correlation between the inputs and prediction error of every output is shown in Figure 7.6. The cross correlation of every input to the residuals is within the 95% confidence interval, indicating that the all process behaviour has been captured.

The estimated model has been tested on a validation data set. The cross correlation between the inputs of the validation set and the model error of the validation set, using the estimated model is shown in Figure 7.7. Here also the cross correlation is within the 95% confidence interval indicating a correctly estimated model.

In Figure 7.8 the output generated by the system simulation is shown together with the output of the identification using the same input. Simulation output is displayed grey and thick, to allow distinction. The estimated model output is almost identical to the simulation output, again indicating a correctly estimation.

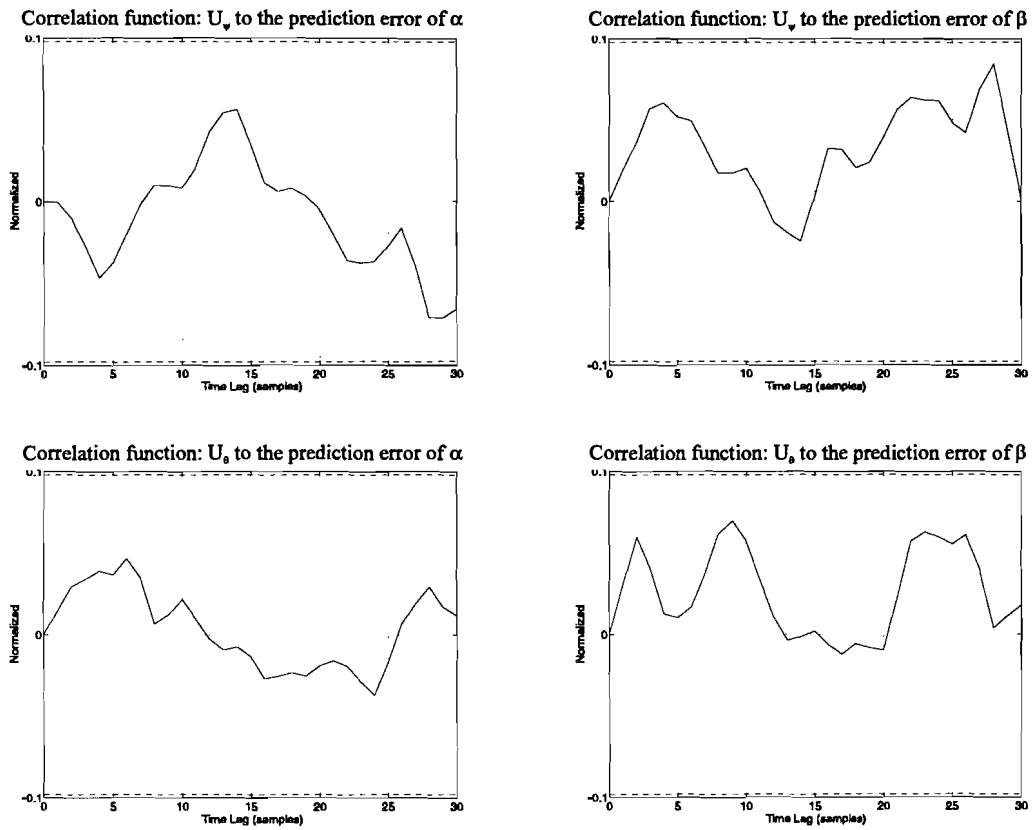


Figure 7.6: Cross correlation between inputs and prediction errors.

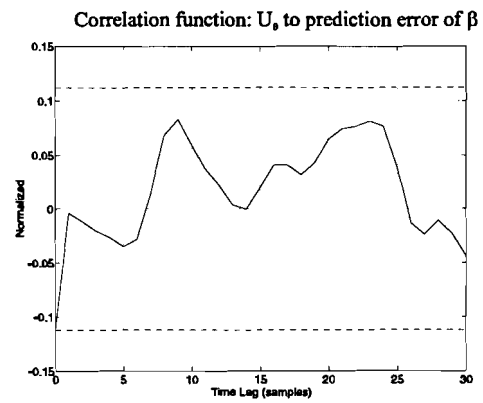
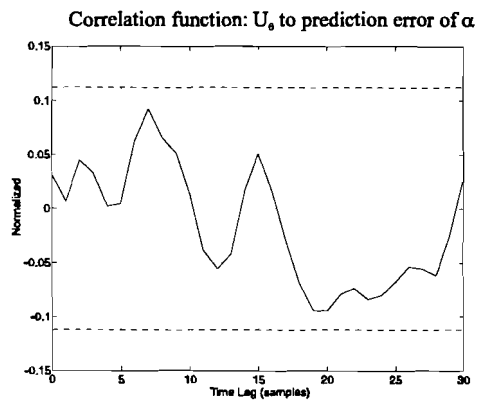
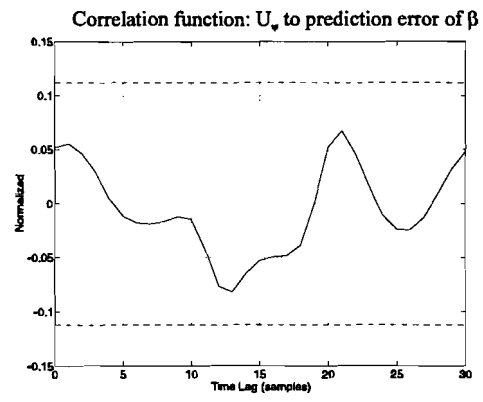
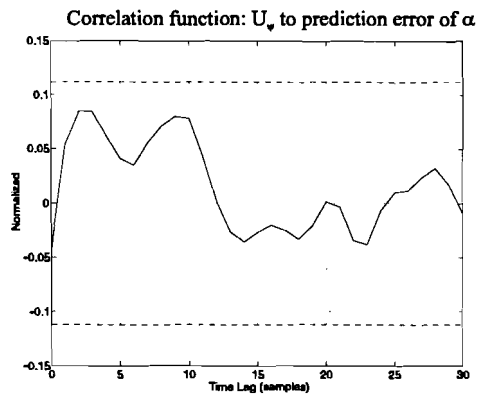


Figure 7.7: Correlation between validation inputs and residuals.



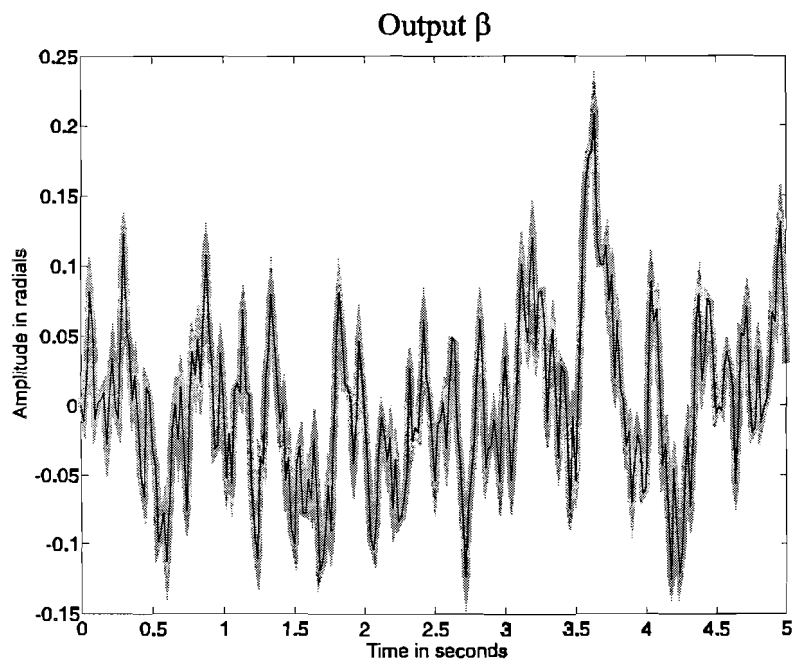
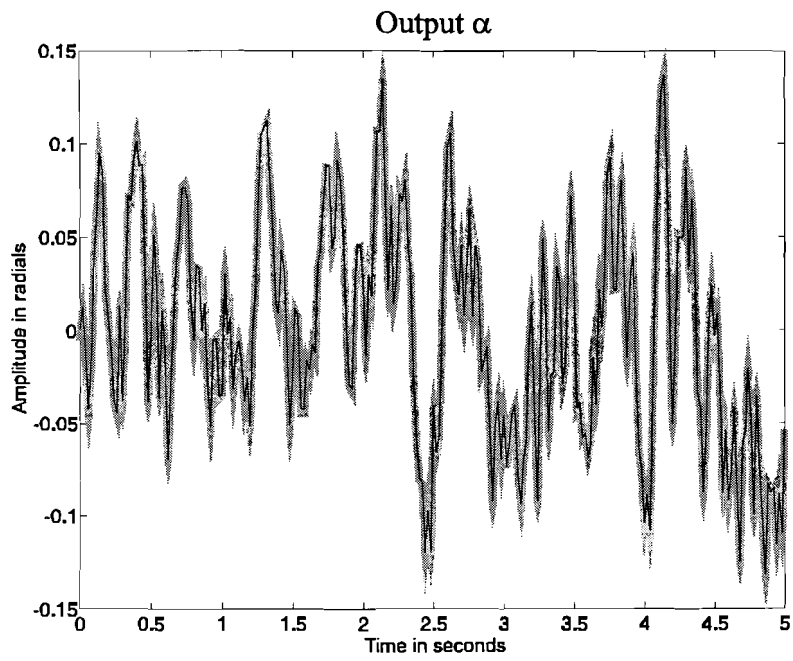


Figure 7.8: System and estimated output.

## 7.4 Siso model validation

It has been shown that the relation between  $U_\psi$  and  $\beta$ , and the relation between  $U_\theta$  and  $\alpha$  are uncorrelated. This indicates that the system can be described by the estimation discarding the  $B_{12}$  and  $B_{21}$  polynomials. This would result in two SISO systems, described by the transfer functions (7.3) and (7.4), omitting the  $B_{12}$  and  $B_{21}$  polynomials.

The check whether these functions describe the system well, the cross-correlation between  $U_\psi$  and the prediction error of  $\alpha$  using the SISO description is calculated. The same is done for  $U_\theta$  and  $\beta$ . The resulting cross-correlation is shown in Figure 7.9.

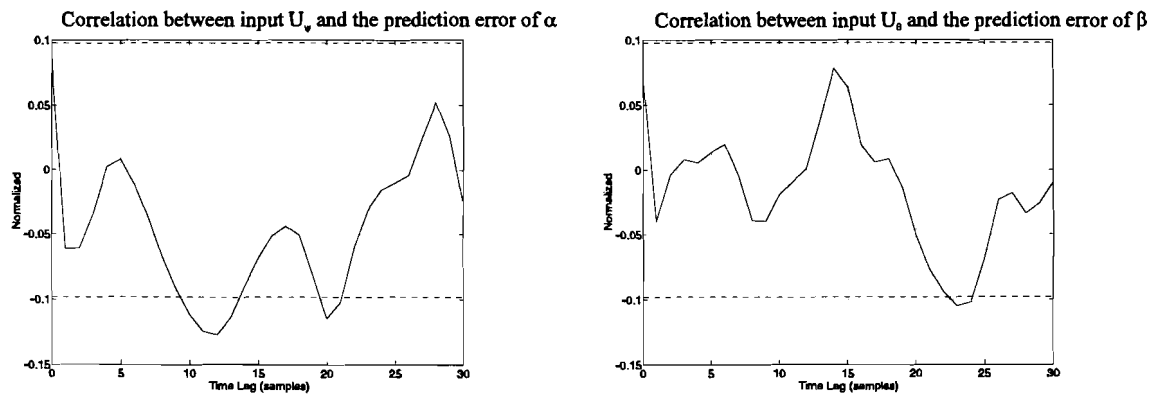


Figure 7.9: Cross correlation between SISO inputs and SISO prediction errors.

It can be seen that the cross-correlation is almost within the 95% confidence interval. This means that the system behaviour can be described reasonably well by the two SISO transfer functions.

The system output and the output of the SISO model is shown in Figure 7.10. The system response is grey. It can be seen that the response is almost identical: the SISO functions describe the system well.

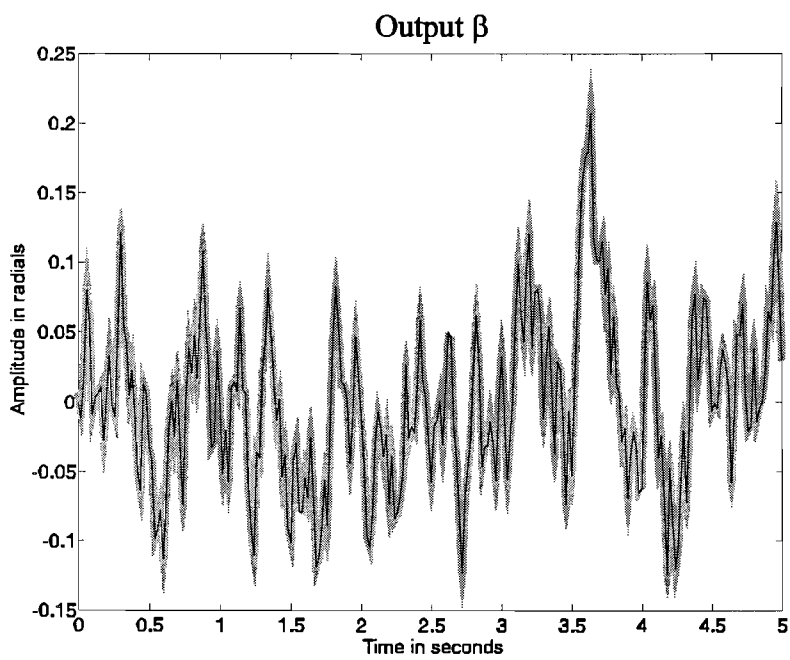
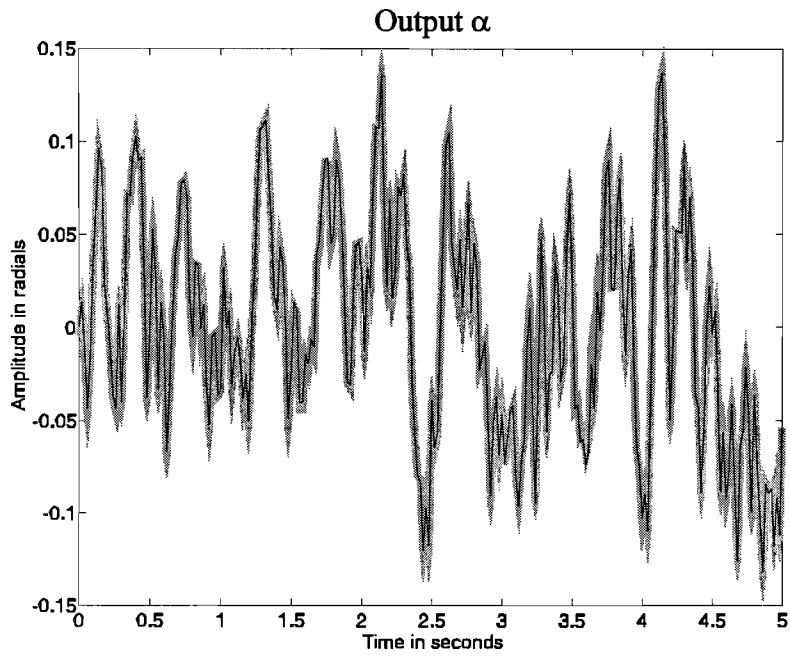


Figure 7.10: SISO response and system response.

## 8. Conclusions

A non-linear model has been developed. The simulation is based on 4 differential equations: 1 for the mirror and 3 for the actuators. The simulation is a qualitative good rendition of the mirror behaviour. However, the characteristics of the cutoff frequency of the simulation and the cutoff frequency of the real system when only  $U_\psi$  or  $U_\theta$  are excited do not correspond. This might be due to the fact that the parameters used in the simulation do not correspond with the those of the real system. By increasing the spring constant of  $C_V$  for instance, the cutoff frequency can be made higher. The parameters will have to be checked with the real system when it comes available again.

The simulation indicates that the system is well damped when voltage control is used. The system has a open loop bandwidth of about 1.25 Hz. A control system can be developed to increase the bandwidth to about the cutoff frequency.

A linear model has been derived from the non-linear differential equations describing the system. The linear model can be transformed into a SISO model with 2 inputs and two outputs. The outputs of the system are the Bryant angles  $\psi$  and  $\theta$ , In the linear case they are the same as the sensor angles  $\alpha$  and  $\beta$ . The linear system does not describe rotations of the mirror around the normal to the mirror surface. In the linear case this rotation can therefore not be controlled.

The bandwidth of the system can be enlarged by increasing the spring constant  $C_V$ . This can be checked by calculating the poles of the linear system. If the bandwidth of the system is not large enough using voltage control, the current control option has to be analyzed. The system is on the edge of instability if current control is used. A controller for current control has to provide the needed stability in this case. If it can be realized, a mixed voltage and current control can be used. This way the damping of the voltage control can be combined with the bandwidth of the current control. The simulation has the option to use voltage control, current control or mixed control.

The sensors of the mirror cannot measure rotation of the mirror round the normal to the mirror surface. This rotation does not directly influence the path of the laser, but it does influence the behaviour of the system, which might indirectly influence the path. A controller for the mirror has to compensate for this influence.

If the rotation round the normal proves to be essential for controlling the mirror, it might be possible to develop a Kalman filter which makes observability possible.

An output error model has been used to identify the system. The inputs and outputs used for the identification are the same as those of the linear model. A second order OE model proves to describe the system well. The poles of the identified system correspond to the slowest poles of the linear model.

There is very little correlation between  $U_\psi$  and  $\beta$ , and between  $U_\theta$  and  $\alpha$ . The MIMO system can reasonably be transformed to 2 SISO systems by discarding the cross polynomials. The system is reasonably described by the SISO models.

## References

- [1] Backx, A.C.P.M. and A.J.W. van den Boom  
TOEGEPASTE SYSTEEMANALYSE  
Eindhoven: Technische Universiteit Eindhoven, 1993.  
Dictaatnr. 5770.
- [2] Boom, A.J.W. van den and A.A.H. Damen  
STOCHASTISCHE SYSTEEM THEORIE  
Eindhoven: Technische Universiteit Eindhoven, 1987.  
Dictaatnr. 5686.
- [3] Bosch, P.P.J. van den and A.C. van der Klauw  
STOCHASTISCHE SYSTEEM THEORIE  
Eindhoven: Technische Universiteit Eindhoven, 1994.  
Dictaatnr. 5686.
- [4] Falkus, H.  
MINIMAL POLYNOMIAL IDENTIFICATION  
USER GUIDE  
Eindhoven: Technische Universiteit Eindhoven 1994.
- [5] Jong, de M.  
ANALYSE VAN EEN 3-D LASERAFBUIGSYSTEEM  
Stageverslag, Eindhoven: Technische Universiteit Eindhoven, 1986.  
Faculteit Werktuigbouwkunde, Vakgroep Fundamentele Werktuigbouwkunde.
- [6] Mathworks  
SIMULAB USER'S GUIDE FOR USE WITH THE MICROSOFT WINDOWS  
SYSTEM  
December 1991
- [7] Sauren, A.  
MULTIBODY DYNAMICA  
Eindhoven: Technische Universiteit Eindhoven, 1986.  
Dictaatnr. 4659.
- [8] Schot, J.A.  
BEGINSELEN DER ELEKTROMECHANICA  
Eindhoven: Technische Universiteit Eindhoven, 1986.  
Dictaatnr. 5672.

## Appendix A: Transforming the local normal coordinates to global coordinates using sensor angles

The normal to the mirror surface  $\underline{n}$  and the sensor angles are shown in Figure A 1, in the global frame.

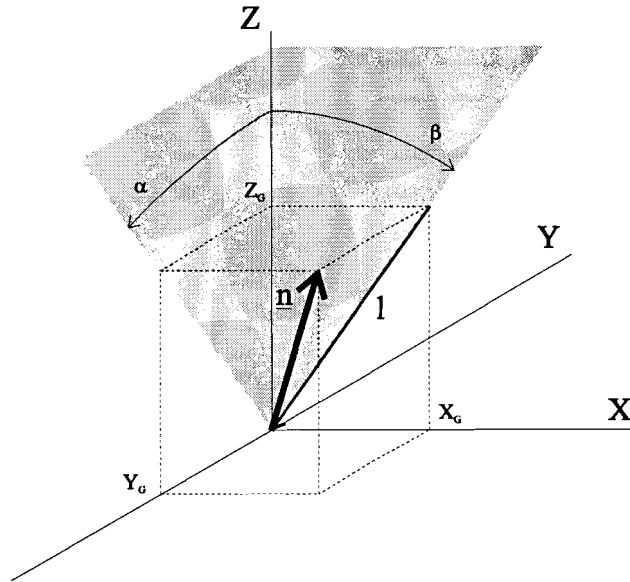


Figure A 1: Mirror normal and sensor angles.

The coordinates  $X_G$  and  $Z_G$  can be given as a function of the length of the xz projection:

$$\begin{aligned} X_G &= l \sin(\beta) \\ Z_G &= l \cos(\beta) \end{aligned} \quad (\text{A.1})$$

Coordinate  $Y_G$  can be found as follows:

$$\begin{aligned} \tan(\alpha) &= \frac{-Y_G}{Z_G} \Rightarrow \\ Y_G &= -l \tan(\alpha) \cos(\beta) \end{aligned} \quad (\text{A.2})$$

This way for  $\underline{n}$  is found:

$$\underline{n} = \begin{bmatrix} X_G \\ Y_G \\ Z_G \end{bmatrix} = \begin{bmatrix} l \sin(\beta) \\ -l \tan(\alpha) \cos(\beta) \\ \cos(\beta) \end{bmatrix} \quad (\text{A.3})$$

The normal has length one, using this we find the value for l:

$$\begin{aligned} \sqrt{(l^2 \sin^2(\beta) + l^2 \cos^2(\beta) + l^2 \tan^2(\alpha) \cos^2(\beta))} &= 1 \Rightarrow \\ l &= \frac{1}{\sqrt{1 + \tan^2(\alpha) \cos^2(\beta)}} \end{aligned} \quad (\text{A.4})$$

Substituting (A 4) in (A 3) we find:

$$\underline{n} = \begin{bmatrix} X_G \\ Y_G \\ Z_G \end{bmatrix} = \frac{1}{\sqrt{1 + \tan^2(\alpha) \cos^2(\beta)}} \begin{bmatrix} \sin(\beta) \\ -\tan(\alpha) \cos(\beta) \\ \cos(\beta) \end{bmatrix} \quad (\text{A.5})$$

## Appendix B: Calculation of $\underline{a}_i$ , $\underline{A}_i$ and $\underline{B}_i$

First the vectors  $\underline{a}_i$  will be calculated in local coordinates:

$$\underline{a}_1 = \begin{bmatrix} x \\ y \\ z \end{bmatrix}_1 = \begin{bmatrix} r \cos(\frac{\pi}{12}) \\ 0 \\ r \sin(\frac{\pi}{12}) \end{bmatrix} \quad (\text{B.1})$$

$$\underline{a}_2 = \begin{bmatrix} x \\ y \\ z \end{bmatrix}_2 = \begin{bmatrix} -r \cos(\frac{\pi}{12}) \sin(\frac{\pi}{6}) \\ r \cos(\frac{\pi}{12}) \cos(\frac{\pi}{6}) \\ r \sin(\frac{\pi}{12}) \end{bmatrix} = \begin{bmatrix} -\frac{1}{2} r \cos(\frac{\pi}{12}) \\ \frac{1}{2} \sqrt{3} r \cos(\frac{\pi}{12}) \\ r \sin(\frac{\pi}{12}) \end{bmatrix} \quad (\text{B.2})$$

$$\underline{a}_3 = \begin{bmatrix} x \\ y \\ z \end{bmatrix}_3 = \begin{bmatrix} -r \cos(\frac{\pi}{12}) \sin(\frac{\pi}{6}) \\ -r \cos(\frac{\pi}{12}) \cos(\frac{\pi}{6}) \\ r \sin(\frac{\pi}{12}) \end{bmatrix} = \begin{bmatrix} -\frac{1}{2} r \cos(\frac{\pi}{12}) \\ -\frac{1}{2} \sqrt{3} r \cos(\frac{\pi}{12}) \\ r \sin(\frac{\pi}{12}) \end{bmatrix} \quad (\text{B.3})$$

Next the vectors  $\underline{A}_i$  will be calculated. The actuator moves along the core. The position of the actuator if  $h_{A_i}=0$  will be defined as the offset position  $\underline{Q}_i$ . The direction of the actuator will be defined as  $\underline{C}_i$ . Subsequently:

$$\underline{A}_i = \underline{Q}_i + h_{A_i} \cdot \underline{C}_i \quad (\text{B.4})$$

For  $\underline{Q}_i$  and  $\underline{C}_i$  can be found:

$$\underline{Q}_1 = \begin{bmatrix} r \cos(\frac{\pi}{12}) + R \sin(\frac{\pi}{12}) \\ 0 \\ r \sin(\frac{\pi}{12}) - R \cos(\frac{\pi}{12}) \end{bmatrix}_G \quad (\text{B.5})$$

$$\underline{Q}_2 = \begin{bmatrix} -\frac{1}{2} \{r \cos(\frac{\pi}{12}) + R \sin(\frac{\pi}{12})\} \\ \frac{1}{2} \sqrt{3} \{r \cos(\frac{\pi}{12}) + R \sin(\frac{\pi}{12})\} \\ r \sin(\frac{\pi}{12}) - R \cos(\frac{\pi}{12}) \end{bmatrix}_G \quad (\text{B.6})$$

$$\underline{Q}_3 = \begin{bmatrix} -\frac{1}{2} \{r \cos(\frac{\pi}{12}) + R \sin(\frac{\pi}{12})\} \\ -\frac{1}{2} \sqrt{3} \{r \cos(\frac{\pi}{12}) + R \sin(\frac{\pi}{12})\} \\ r \sin(\frac{\pi}{12}) - R \cos(\frac{\pi}{12}) \end{bmatrix}_G \quad (\text{B.7})$$

$$\underline{C}_1 = \frac{\underline{a}_1 - \underline{A}_1}{\|\underline{a}_1 - \underline{A}_1\|_2} \Big|_{\text{Equilibrium}} = \begin{bmatrix} -\sin(\frac{\pi}{12}) \\ 0 \\ \cos(\frac{\pi}{12}) \end{bmatrix}_G \quad (\text{B.8})$$

$$\underline{C}_2 = \frac{\underline{a}_2 - \underline{A}_2}{\|\underline{a}_2 - \underline{A}_2\|_2} \Big|_{\text{Equilibrium}} = \begin{bmatrix} \frac{1}{2} \sin(\frac{\pi}{12}) \\ -\frac{1}{2} \sqrt{3} \sin(\frac{\pi}{12}) \\ \cos(\frac{\pi}{12}) \end{bmatrix}_G \quad (\text{B.9})$$



$$C_3 = \frac{a_3 - A_3}{\|a_i - A_i\|_2} \Big|_{\text{Equilibrium}} = \begin{bmatrix} \frac{1}{2} \sin(\frac{\pi}{12}) \\ \frac{1}{2} \sqrt{3} \sin(\frac{\pi}{12}) \\ \cos(\frac{\pi}{12}) \end{bmatrix}_G \quad (\text{B.10})$$

If the Bryant angles are known, the vectors  $\underline{\Delta}_i$  can be calculated in local coordinates.

For the vectors  $\underline{B}_i$  can be found:

$$\underline{B}_i = -\underline{C}_i \cdot \underline{Q} + \underline{a}_i \quad (\text{B.11})$$

This results in:

$$\begin{aligned} \underline{B}_1 &= \underline{Q} \cdot \begin{bmatrix} \sin(\frac{\pi}{12}) \\ 0 \\ -\cos(\frac{\pi}{12}) \end{bmatrix} + \begin{bmatrix} r \cos(\frac{\pi}{12}) \\ 0 \\ r \sin(\frac{\pi}{12}) \end{bmatrix} \\ \underline{B}_2 &= \underline{Q} \begin{bmatrix} -\frac{1}{2} \sin(\frac{\pi}{12}) \\ \frac{1}{2} \sqrt{3} \sin(\frac{\pi}{12}) \\ -\cos(\frac{\pi}{12}) \end{bmatrix} + \begin{bmatrix} -\frac{1}{2} r \cos(\frac{\pi}{12}) \\ \frac{1}{2} \sqrt{3} r \cos(\frac{\pi}{12}) \\ r \sin(\frac{\pi}{12}) \end{bmatrix} \\ \underline{B}_3 &= \underline{Q} \begin{bmatrix} -\frac{1}{2} \sin(\frac{\pi}{12}) \\ -\frac{1}{2} \sqrt{3} \sin(\frac{\pi}{12}) \\ -\cos(\frac{\pi}{12}) \end{bmatrix} + \begin{bmatrix} -\frac{1}{2} r \cos(\frac{\pi}{12}) \\ -\frac{1}{2} \sqrt{3} r \cos(\frac{\pi}{12}) \\ r \sin(\frac{\pi}{12}) \end{bmatrix} \end{aligned} \quad (\text{B.12})$$

## Appendix C: The simulation blocks

The mirror dynamics are grouped in a block called "Mirror". This block contains the system dynamics, using three inputs. The inputs can be the voltages or the currents on the actuators, dependent on whether voltage or current control is used. Before the simulation can be started certain parameters should be set in the Matlab workspace. The parameters to be set are:

- $C_v$  Spring constant of pretensioning spring. (Used value :40)
- $C_s$  Spring constant of string. (Value used: 1.5e5)
- $D$  Damping of actuator. (Value used: 0)
- $M$  Mass of actuator. (Value used: 9.5e-3)
- $J$  Inertia of mirror. (Value used: 5.6e-8)
- $L$  Inductance of actuator coil. (Value used: 1e-3)
- $R$  Resistance of actuator coil. (Value used: 3.5)
- $A$  Actuator constant. (Value used: 3.16)
- $F_0$  Pretensioning force. (Value used: 0)
- $VC$  Parameter indicating whether Voltage Control or current control is used. For voltage control set this parameter to 1, for current control set this value to 0. "Mixed" control can be achieved by assigning a value between 0 and 1.

The parameters can easily be set in the Matlab workspace, or using the initialization file MIRINI.M.

If the group mirror is opened the simulation layout can be seen. In the group layout can be seen. Only one group "Momentum on arm 1 (local)" is shown in the diagram. The group mirror also contains the groups "Momentum on arm 2 (local)" and "Momentum on arm 3

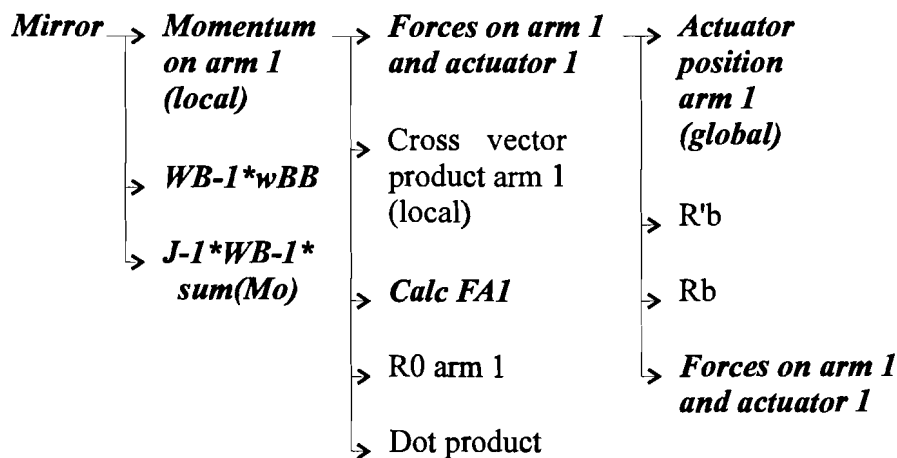


Figure A 2: Layout of the simulation .

(local)" but they are omitted for clarity.

The layout shows how the groups are incorporated in other groups. The groups marked bold italic are displayed below.

The function of every group is listed below.

- **Mirror**: total mirror simulation. The inputs are the 3 actuator inputs, the outputs are the Bryant angles.

- **Momentum on arm1 (local)**: calculates the force on mirror arm 1 as a function of the Bryant angles and of the actuator position in local coordinates. The same goes for the other "Momentum on armi (local)" groups.
- **WB-1\*wBB**: calculates  $W_B^{-1} \dot{\omega}_{BB}$ .
- **J-1\*WB-1\*sum(Mo)**: calculates  $j_0^{-1} W_B^{-1} M_0$ .
- **Forces on arm1 and actuator1**: calculates the forces on arm 1 and actuator 1. The force on the arm is calculated in local coordinates, the force on the actuator is calculated in global variables.
- **Calc FA1**: calculates the actuator force  $F_A$  for current and voltage control.
- **Actuator position arm1 global**: calculates the actuator position  $h_A$  along the core.
- **Forces on arm1 and actuator1 (local)**: calculates the forces on the actuator and the mirror arm both in local coordinates.

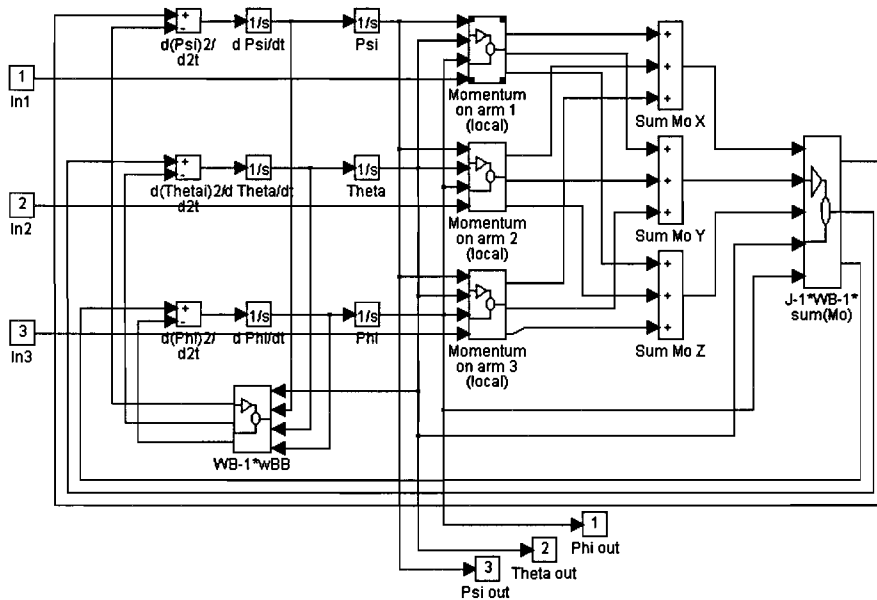


Figure A 3: Simulink block Mirror.

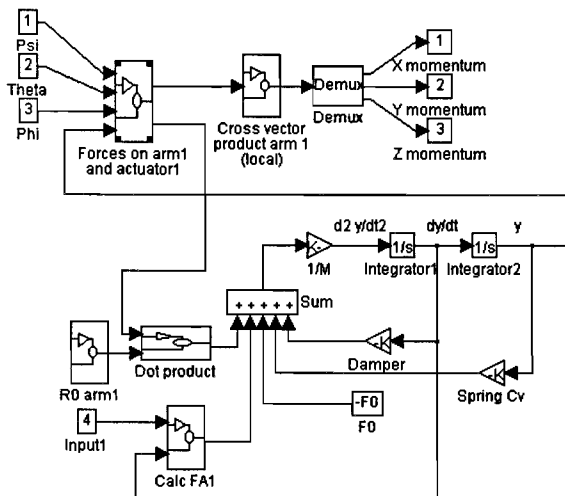


Figure A 4: Simulink block Momentum on arm1 (local).

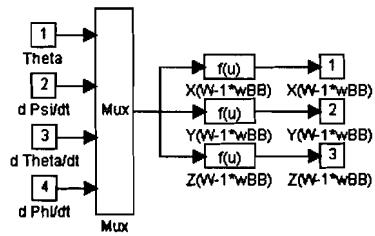


Figure A 5: Simulink block WB-1\*wBB.

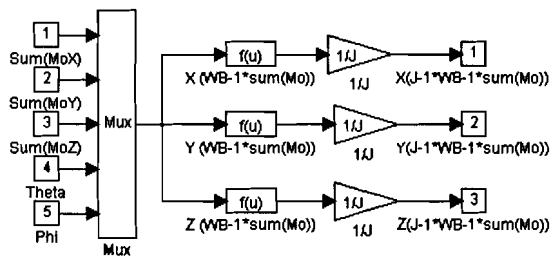


Figure A 6: Simulink block J-1\*WB-1 sum(Mo).

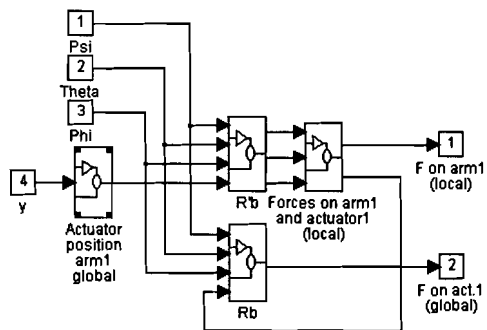


Figure A 7: Simulink block Forces on arm1 and actuator1.

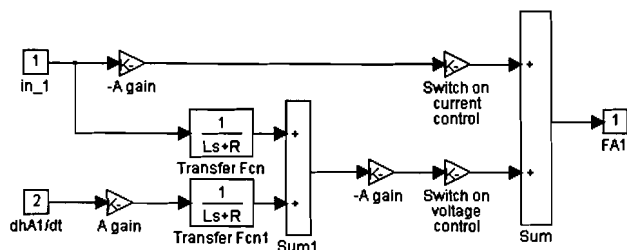


Figure A 8: Simulink block Calc FA1.

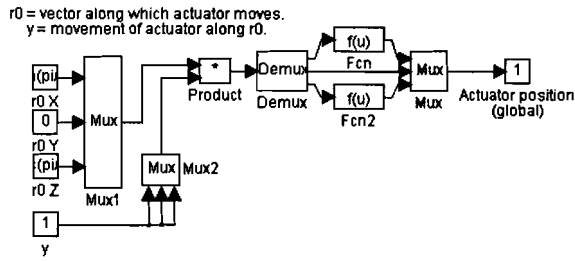


Figure A 9: Simulink block Actuator position global.

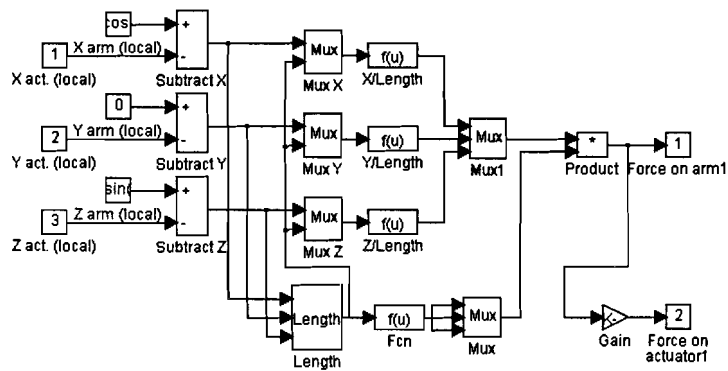


Figure A 10: Simulink block Forces on arm1 and actuator1 (local).

## Appendix D: Notes on running simulations in Simulink

The simulation of the system is more 'stable' when voltage control is used. This can be verified by looking at the bode and step responses of the linearized model. This can also be seen by the fact that there is no damping in the system when current control is used, and there is a considerable damping due to the induction voltage when voltage control is used.

Due to the great stiffness of the string very small time steps must be taken while simulating. In this section a few notes on how to use the simulation are described.

- The algorithm used for the simulations done in this research work is the Runga Kutta 4/5 method.
- If voltage control is used, time steps of about  $1 \cdot 10^{-5}$  need to be used. When current control is used, time steps as little as  $1 \cdot 10^{-7}$  need to be used.
- An indication of whether the simulation is giving an accurate result is by monitoring the string force of the actuators. If the string force shows an oscillation in *every* time step, it means that the time step is too large. The time step should be made smaller.
- Regarding the settings in the parameter section of the simulation menu:  
The minimum time step is the smallest time step the simulation is allowed to make to achieve the tolerance. If the tolerance can not be achieved using the minimum time step, then the minimum time step will still be used, though the tolerance is not achieved. The maximum value is the largest time step the simulation is allowed to take, even if the tolerance is achieved. If the tolerance can be achieved with a larger time step than the maximum time step, still the maximum time step will be used. Time steps are varied during the simulation between the maximum and minimum time step, using the largest possible time step to achieve the tolerance.
- If a simulation is run for identification purposes, the time step usually needs to be constant for use with the identification algorithm. This can be achieved by giving minimum and maximum time step the same value. This value should be chosen so that the simulation is accurate through the whole simulation.
- When small time steps are used, large amounts of data are generated. If all this data is to be stored in the computer's memory the system can slow down dramatically due to the fact that it is constantly swapping to the hard drive, or run out of memory altogether. To avoid this it is best to write data to disk during the simulation. A Simulink block is available for this purpose. Beware to not store too many variables in one file, because if too many variables are stored in one file, the file might become too large to read. To avoid this, store all variables in different files.
- All variables are stored with the time vector. This means that every file saved contains the time vector, which is as large as the variable vector. Storing variables unnecessary in different files will cost valuable disk space, due to the fact that the time vector is saved several times. Consideration should therefore be taken whether to save variables in one file or in different files.
- Usually the time steps used by the simulation are smaller than the time steps necessary for further manipulation of the data. To save disk space and to increase processing time considerably it is better to reduce the data immediately once the simulation is done.

## Appendix E: Matlab M-files

### MIRINLM

```
% initialize mirror model
% Cv= Spring constant of actuator spring
% D= Damper actuator
% M= Mass actuator
% F0= Force on actuator due to pretensioning of Cv
% Cs= Spring constant of arm-actuator connection
% J= Inertia mirror
% A= Coil gain
% L= Coil inductance
% R= Coil resistance
% VC Supply control parameter.
% VC=1 Indicates voltage control
% VC=0 Indicates current control
```

```
clear
pack
Cv=40;
D=0;
M=9.5e-3;
F0=0;
Cs=1.5e5;
A=3.16;
J=5.6e-8;
L=1e-3;
R=3.5;
VC=1;
```

### CAALFAV.M

```
%calculate denominator for voltage control

V=-(3/8)*7e-3+1.5e-3*(7/25)*sin(pi/12)*sin(pi/12);
s5=J*M*L;
s4=J*(D*L+M*R);
s3=J*(D*R+L*(Cv+Cs)+A*A)+F0*V*M*L+1.5*4.9e-5*Cs*M*L;
s2=J*R*(Cv+Cs)+F0*V*(D*L+M*R)+1.5*4.9e-5*Cs*(M*R+D*L);
s1=F0*V*(D*R+L*(Cv+Cs)+A*A)+1.5*4.9e-5*Cs*(R*D+Cv*L+A*A);
s0=F0*V*R*(Cv+Cs)+1.5*4.9e-5*R*Cv*Cs;
den=[s5 s4 s3 s2 s1 s0];

%calculate numerator for voltage control

num=[0 0 0 0 0 .5*sqrt(3)*7e-3*Cs*A];
```

### CAALFAI.M

%calculate denominator for voltage control

```
V=-(3/8)*7e-3+1.5e-3*(7/25)*sin(pi/12)*sin(pi/12);
clear num den;
s4=J*M;
s3=J*D;
s2=J*(Cv+Cs)+F0*V*M+1.5*4.9e-5*Cs*M;
s1=F0*V*D+1.5*4.9e-5*Cs*D;
s0=F0*V*(Cv+Cs)+1.5*4.9e-5*Cv*Cs;
den=[s4 s3 s2 s1 s0];
```

%calculate numerator for voltage control

```
num=[0 0 0 0.5*sqrt(3)*7e-3*Cs*A];
```

### CABETA.V.M

%calculate denominator for voltage control

```
V=-(3/8)*7e-3+1.5e-3*(7/25)*sin(pi/12)*sin(pi/12);
clear num den;
s5=J*M*L;
s4=J*(D*L+M*R);
s3=J*(D*R+L*(Cv+Cs)+A*A)+F0*V*M*L+1.5*4.9e-5*Cs*M*L;
s2=J*R*(Cv+Cs)+F0*V*(D*L+M*R)+1.5*4.9e-5*Cs*(M*R+D*L);
s1=F0*V*(D*R+L*(Cv+Cs)+A*A)+1.5*4.9e-5*Cs*(R*D+Cv*L+A*A);
s0=F0*V*R*(Cv+Cs)+1.5*4.9e-5*R*Cv*Cs;
den=[s5 s4 s3 s2 s1 s0];
```

%calculate numerator for voltage control

```
num=[0 0 0 0 7e-3*Cs*A];
```

### CABETA.I.M

%calculate denominator for voltage control

```
V=-(3/8)*7e-3+1.5e-3*(7/25)*sin(pi/12)*sin(pi/12);
clear num den;
s5=J*M*L;
s4=J*(D*L+M*R);
s3=J*(D*R+L*(Cv+Cs)+A*A)+F0*V*M*L+1.5*4.9e-5*Cs*M*L;
s2=J*R*(Cv+Cs)+F0*V*(D*L+M*R)+1.5*4.9e-5*Cs*(M*R+D*L);
s1=F0*V*(D*R+L*(Cv+Cs)+A*A)+1.5*4.9e-5*Cs*(R*D+Cv*L+A*A);
s0=F0*V*R*(Cv+Cs)+1.5*4.9e-5*R*Cv*Cs;
den=[s5 s4 s3 s2 s1 s0];
```

%calculate numerator for voltage control



```
num=[0 0 0 0 0 7e-3*Cs*A];
```

### **ADNOISE.M**

```
function[signal]=adnoise(signal,S2N);
```

```
% function[signal]=adnoise(signal,S2N);
```

```
%
```

```
% Add normally distributed noise to a vector
```

```
% Signal to noise ratio: S2N
```

```
% Where S2N is the power ratio in dB ( $10 \cdot \log_{10}(\text{signal power}/\text{noise power})$ )
```

```
randn('seed',sum(100*clock));
```

```
% generate a 'random' seed
```

```
e=randn(size(signal));
```

```
% generate a normally distributed noise signal
```

```
sigdev=real(std(signal));
```

```
% calculate standard deviation of signal vector
```

```
noise=e*(sigdev/std(e))*10^(-S2N/20);
```

```
% calculate noise;
```

```
%  $10 \cdot \log_{10}(\text{sigdev}^2/(\text{std}(\text{noise}))^2)$ 
```

```
% calculate actual signal to noise ratio
```

```
signal=signal+noise;
```

```
% add noise to signal
```